

Article

Acid Ceramidase Inhibitor LCL-805 Antagonizes Akt Signaling and Promotes Iron-Dependent Cell Death in Acute Myeloid Leukemia

Johnson Ung ^{1,*}, Su-Fern Tan ^{2,3}, Todd E. Fox ^{2,4}, Jeremy J. P. Shaw ², Maansi Taori ², Bethany J. Horton ⁵, Upendarrao Golla ⁶, Arati Sharma ^{7,8}, Zdzislaw M. Szulc ⁹, Hong-Gang Wang ⁸, Charles E. Chalfant ^{2,3,10}, Myles C. Cabot ^{11,12}, David F. Claxton ^{6,8}, Thomas P. Loughran, Jr. ^{2,3} and David J. Feith ^{2,3,*}

¹ Department of Microbiology, Immunology and Cancer Biology, University of Virginia School of Medicine, Charlottesville, VA 22908, USA

² Department of Medicine, Division of Hematology & Oncology, University of Virginia School of Medicine, Charlottesville, VA 22908, USA; st4ub@virginia.edu (S.-F.T.); tef3b@virginia.edu (T.E.F.); jjs3ge@virginia.edu (J.J.P.S.); tpq4ew@virginia.edu (M.T.); cechalfant@virginia.edu (C.E.C.); tl7cs@uvahealth.org (T.P.L.J.)

³ University of Virginia Cancer Center, University of Virginia School of Medicine, Charlottesville, VA 22908, USA

⁴ Department of Pharmacology, University of Virginia School of Medicine, Charlottesville, VA 22908, USA

⁵ Department of Public Health Sciences, Division of Translational Research and Applied Statistics, University of Virginia School of Medicine, Charlottesville, VA 22908, USA; bjh8f@virginia.edu

⁶ Department of Medicine, Division of Hematology and Oncology, Pennsylvania State University College of Medicine, Hershey, PA 17033, USA; ugolla@pennstatehealth.psu.edu (U.G.); dclaxton@pennstatehealth.psu.edu (D.F.C.)

⁷ Department of Pharmacology, Pennsylvania State University College of Medicine, Hershey, PA 17033, USA; asharma@pennstatehealth.psu.edu

⁸ Penn State Cancer Institute, Pennsylvania State University College of Medicine, Hershey, PA 17033, USA; hwang3@pennstatehealth.psu.edu

⁹ Department of Biochemistry and Molecular Biology, Medical University of South Carolina College of Medicine, Charleston, SC 29425, USA; szulcz@muscc.edu

¹⁰ Research Service, Richmond Veterans Administration Medical Center, Richmond, VA 23249, USA

¹¹ East Carolina Diabetes and Obesity Institute, East Carolina University, Greenville, NC 27858, USA; cabotm@ecu.edu

¹² Department of Biochemistry & Molecular Biology, Brody School of Medicine, East Carolina University, Greenville, NC 27834, USA

* Correspondence: ju7a@virginia.edu (J.U.); djf2g@virginia.edu (D.J.F.); Tel.: +1-434-982-2187 (J.U.); +1-434-243-8067 (D.J.F.)



Citation: Ung, J.; Tan, S.-F.; Fox, T.E.; Shaw, J.J.P.; Taori, M.; Horton, B.J.; Golla, U.; Sharma, A.; Szulc, Z.M.; Wang, H.-G.; et al. Acid Ceramidase Inhibitor LCL-805 Antagonizes Akt Signaling and Promotes Iron-Dependent Cell Death in Acute Myeloid Leukemia. *Cancers* **2023**, *15*, 5866. <https://doi.org/10.3390/cancers15245866>

Academic Editor: Jonas Cicenas

Received: 21 October 2023

Revised: 28 November 2023

Accepted: 30 November 2023

Published: 15 December 2023



Copyright: © 2023 by the authors. Licensee MDPI, Basel, Switzerland. This article is an open access article distributed under the terms and conditions of the Creative Commons Attribution (CC BY) license (<https://creativecommons.org/licenses/by/4.0/>).

Simple Summary: The lysosomal lipid hydrolase acid ceramidase is upregulated in acute myeloid leukemia and promotes leukemic blast survival, underscoring its potential for therapeutic targeting. B-13 is an established ceramidase inhibitor with demonstrated efficacy in multiple solid cancers. Next-generation lysosome-localizing prodrugs of B-13 have been developed but have not been evaluated in AML. This study characterizes the in vitro anti-leukemic efficacy and cell death mechanisms of the B-13 analog and acid ceramidase inhibitor LCL-805 in acute myeloid leukemia.

Abstract: Acute myeloid leukemia (AML) is an aggressive hematologic malignancy requiring urgent treatment advancements. Ceramide is a cell-death-promoting signaling lipid that plays a central role in therapy-induced cell death. We previously determined that acid ceramidase (AC), a ceramide-depleting enzyme, is overexpressed in AML and promotes leukemic survival and drug resistance. The ceramidase inhibitor B-13 and next-generation lysosomal-localizing derivatives termed dimethylglycine (DMG)-B-13 prodrugs have been developed but remain untested in AML. Here, we report the in vitro anti-leukemic efficacy and mechanism of DMG-B-13 prodrug LCL-805 across AML cell lines and primary patient samples. LCL-805 inhibited AC enzymatic activity, increased total ceramides, and reduced sphingosine levels. A median EC50 value of 11.7 μ M was achieved for LCL-805 in cell viability assays across 32 human AML cell lines. As a single agent tested across a panel

of 71 primary AML patient samples, a median EC50 value of 15.8 μ M was achieved. Exogenous ceramide supplementation with C6-ceramide nanoliposomes, which is entering phase I/II clinical trial for relapsed/refractory AML, significantly enhanced LCL-805 killing. Mechanistically, LCL-805 antagonized Akt signaling and led to iron-dependent cell death distinct from canonical ferroptosis. These findings elucidated key factors involved in LCL-805 cytotoxicity and demonstrated the potency of combining AC inhibition with exogenous ceramide.

Keywords: acute myeloid leukemia; sphingolipids; acid ceramidase; ceramide; dimethylglycine-B-13 prodrug; LCL-805; C6-ceramide nanoliposome; Akt; iron chelation

1. Introduction

Acute myeloid leukemia (AML) is an aggressive, heterogenous malignancy that afflicts tens of thousands of people annually [1]. Characterized by the clonal expansion of immature myeloid blasts, clinical features of AML include pancytopenia, anemia, and bone marrow failure [2]. Although individuals of all ages develop AML, the median age at diagnosis is 65 [3]. Intensive induction chemotherapy has been the primary treatment option since the 1970s, with several targeted therapeutics approved in the 2010s [4]. Despite these approvals to supplement chemotherapy, poor treatment responses and high relapse rates persist. Moreover, treatment options are limited for elderly individuals who are unable to tolerate intensive induction chemotherapy.

Ceramides reside at the putative center of the complex sphingolipid metabolic pathway. Ceramide levels increase in response to chemotherapy [5], radiation [6], or targeted therapeutics [7] and contribute to treatment-induced cytotoxicity [8]. Multiple enzymes catabolize ceramide or modify its structure to generate increasingly complex sphingolipids. These metabolic paths reduce the ceramide pool to promote leukemia survival and drug resistance [9]. The development of ceramide-generating therapeutics is an enticing anti-neoplastic strategy as ceramides are important mediators of cell death, and cancer cells modulate ceramide catabolism to maintain survival. Elevating intracellular ceramides through exogenous supplementation [10,11] or metabolic blockade [12,13] is actively being explored as an anticancer therapy.

Aberrant sphingolipid metabolism is well documented in AML [14]. Our group previously identified and validated acid ceramidase (AC) as a therapeutic target [12]. AC is a lysosomal lipid hydrolase that catabolizes ceramides into sphingosine and free fatty acids. AC overexpression in AML is associated with and promotes chemotherapy resistance [15,16]. Moreover, high AC activity is associated with poorer survival in patients who received induction chemotherapy [17]. AC targeting has been extensively studied in solid cancers with several inhibitors in preclinical development [18,19]. B-13 is a ceramidase inhibitor with demonstrated cytotoxicity in multiple solid cancers [20,21]. Unfortunately, the neutrophilic properties of B-13 preclude its accumulation in the lysosome where AC resides. To overcome this hurdle, next-generation lysosome-localizing B-13 analogs termed dimethylglycine (DMG)-B-13 prodrugs were developed [22].

In the present study, we characterized the *in vitro* anti-leukemic efficacy and mechanisms of a DMG-B-13 prodrug, LCL-805, in AML for the first time. Our findings demonstrated that LCL-805 is an effective AC inhibitor and is cytotoxic toward AML cell lines and patient samples. LCL-805 cytotoxicity was further amplified via C6-ceramide nanoliposome (CNL) supplementation. Mechanistically, LCL-805 inhibited Akt signaling and induced iron-dependent cell death distinct from canonical ferroptosis.

2. Materials and Methods

2.1. Reagents

Inhibitors used for rescue studies: zVAD-FMK (Selleck Chemicals, Houston, TX, USA, #S7023); chloroquine (Selleck Chemicals, #S6999); bafilomycin A1 (Selleck Chemicals,

#S1413); SC-79 (Cayman, Ann Arbor, MI, USA, #14972A); deferoxamine mesylate (Selleck Chemicals, #S5742); liproxstatin-1 (Selleck Chemicals, #S7699); ferrostatin-1 (Selleck Chemicals, #S7243); GSK'872 (Selleck Chemicals, #S8465); necrostatin-1 (Selleck Chemicals, #S8037); pepstatin A (Cayman, #9000469); and CA-074me (Selleck Chemicals, #S7420).

Anti-acid ceramidase antibody (#612302) was obtained from BD Transduction Laboratories (Franklin Lakes, NJ, USA). The following antibodies were obtained from Cell Signaling Technologies (Danvers, MA, USA): caspase-3 (#9662); PARP (#9542); Mcl-1 (#5453); Bcl-2 (#4223); Bcl-xL (#2764); XIAP (#2042); LC3A (#4599); phospho-Akt (Ser473; #4060); Pan Akt (#4691); GPX4 (#52455); HIF-1 α (#14179); β -actin (#3700); anti-rabbit IgG, HRP-linked (#7074); and anti-mouse IgG, HRP-linked (#7076).

2.2. Cell Culture

Cell lines were cultured in a 37 °C humidified incubator at 5% CO₂. All cell lines were utilized within 6–8 weeks of thawing. OCI-AML3 was cultured in RPMI-1640 (Corning, #10-040) supplemented with 15% FBS (VWR, Radnor, PA, USA, #97068–085). MOLM-16, F-36p, SKM-1, ME-1, SET-2, Kasumi-1, Kasumi-3, and Kasumi-6 were cultured in RPMI-1640 supplemented with 20% FBS. KG-1, KG-1/ABT737R, KG-1a, and KG-1a/ABT737R were cultured in IMDM (ThermoFisher, Waltham, MA, USA, #12440) supplemented with 20% FBS. MV4-11 was cultured in IMDM supplemented with 10% FBS. OCI-AML4 was cultured in α -MEM (ThermoFisher, #12571063) supplemented with 20% FBS. Some cell lines required additional hGM-CSF supplementation (Miltenyi Biotec, Gaithersburg, MD, USA, #130–095-372): OCI-AML4 (100 ng/mL); F-36p, SKNO-1, and Kasumi-6 (10 ng/mL); and TF-1 (2 ng/mL). All remaining cell lines were cultured in RPMI-1640 supplemented with 10% FBS.

Drug-resistant cell lines were maintained in the presence of their respective drugs during routine cell culture. HL-60/VCR [23] were supplemented with 1 μ g/mL vincristine sulfate (Cayman, #11764). ABT737 (Cayman, #11501) was supplemented to ABT737R cell lines: HL-60/ABT737R [24] (5 μ M ABT737); KG-1/ABT737R and KG-1a/ABT737R [24] (1 μ M ABT737).

Cell lines obtained from DSMZ include SKNO-1, OCI-M2, and SKM-1. All remaining cell lines were gifted (see acknowledgments) or acquired from ATCC. Short tandem repeat DNA profiling (LabCorp, Burlington, NC, USA, formerly known as Genetica Cell Line Testing) was utilized to authenticate cell lines. All cell lines were confirmed negative for mycoplasma contamination using the MycoAlert PLUS kit (Lonza, Morristown, NJ, USA, #LT07–710). Non-targeting control (NT CT), ATG5 knockout (ATG5KO), and ATG7 knockout (ATG7KO) gene-edited MV4-11 cells were generated as previously described [25].

Detailed mechanistic studies utilized MM-6 and OCI-AML2, which were chosen as established human AML cell lines that represent two different subtypes of AML (MM-6 = acute monocytic leukemia, AML FAB M5; OCI-AML2 = acute myeloid leukemia, AML FAB M4) with differing mutations, cytogenetics, and responses to LCL-805.

2.3. Primary AML Patient Samples and Healthy Normal Samples

AML patient samples were collected with informed consents signed for sample collection according to approved protocols by the institutional review boards of the Milton S. Penn State Hershey Medical Center and the University of Virginia School of Medicine and in accordance with the Declaration of Helsinki (Supplemental Table S1). Normal peripheral blood mononuclear cells (PBMCs) and bone marrow (BM) cells were purchased from AllCells (Alameda, CA, USA), Virginia Blood Services, Zen-Bio (Durham, NC, USA), and Inova Blood Donor Services (Sterling, VA, USA). PBMCs and BM mononuclear cells were isolated from patients' whole blood using the Ficoll-Paque gradient separation method and cryopreserved. Cryopreserved normal and AML patient PBMC samples were thawed and resuspended in RPMI growth medium with 15% FBS. Cell viability was determined using Muse Count & Viability Kit (Cytex, Fremont, CA, USA, #MCH100102).

2.4. LCL-805 Synthesis

LCL-805, dimaleate salt of (1R,2R)-2-N-(tetradecanoylamino)-1-(4'-nitrophenyl)-propyl-1,3-O-di-(N,N-dimethylamino) acetate, was prepared according to the previously published method from (1R,2R)-2-N-(tetradecanoylamino)-1-(4'-nitrophenyl)-propyl-1,3-diol and N,N-dimethylamino glycine, where in lieu of hydrochloric acid, maleic acid was applied in the final step [22].

2.5. Ceramide Nanoliposome (CNL) Formulation

Lipids, in chloroform, were combined at 3.75:1.75:0.75:0.75:3.0 molar ratio consisting of 1,2-dioleoyl-sn-glycero-3-phosphocholine/1,2-dioleoyl-sn-glycero-3-phosphoethanolamine/1,2-distearoyl-sn-glycero-3-phosphoethanolamine-N-[methoxy PEG(2000)]/PEG(750)-C8-ceramide/C6-ceramide. Lipids were dried under a stream of nitrogen gas. Lipids were subsequently hydrated with sterile 0.9% NaCl solution, sonicated, and underwent extrusion through 100 nm polycarbonate membranes at 60 °C. CNL was sonicated in a 37 °C water bath for 10–15 min before use.

2.6. Acid Ceramidase (AC) Activity Assay

A total of 20,000 cells were seeded onto black 96-well assay plates (Corning, NY, USA, #3603). LCL-805 was prepared by diluting 1:10 in 37 °C RPMI-1640 supplemented with 10% FBS. Cells were treated with vehicle (DMSO) or LCL-805 at the indicated concentrations in a final volume of 50 µL and incubated for the indicated times. After LCL-805 treatment, 50 µL of the AC substrate, RBM14C12 (Avanti Polar Lipids, Alabaster, AL, USA, #860855), was prepared in RPMI-1640 supplemented with 10% FBS and added to the cells at a final concentration of 16 µM and incubated for 3 h. After incubation, 50 µL of 100% methanol was added, followed immediately with 100 µL of 2.5 mg/mL sodium periodate in 100 mM glycine, pH 10.6. The plates were incubated for 2 h at 37 °C. After incubation, fluorescence was measured using the Synergy HT plate reader (Biotek, Winooski, VT, USA; gain = auto; 365 nm excitation/410–460 nm emission). Following background subtraction, fluorescence was normalized to vehicle control, which was defined as 100%.

2.7. Immunoblotting

Cells were seeded between 5×10^5 and 1×10^6 cells/mL and treated with the indicated concentrations for the indicated timepoints. Following treatment, cells were pelleted, washed in 1X PBS, pelleted, resuspended in 1X RIPA buffer (Sigma, St. Louis, MO, USA, #R0278-500ML) supplemented with a protease inhibitor cocktail (Sigma, #P8340), phosphatase inhibitor cocktail 2 (Sigma, #P5726), and phosphatase inhibitor cocktail 3 (Sigma, #P0044), vortexed, and incubated on ice for 30 min. Samples were centrifuged at $16,000 \times g$ for 10 min at 4 °C. Supernatant was collected and stored at –80 °C. Protein levels were quantified using the bicinchoninic acid (BCA) protein assay kit (Pierce, Waltham, MA, USA, #23225) following the manufacturer's protocol. Samples were prepared in sample buffer (Invitrogen, Waltham, MA, USA #NP0007) and reducing agent (Invitrogen, #NP0009), denatured at 90 °C for 10 min, centrifuged, and cooled at 4 °C. Protein samples were resolved on 4–12% Bis-Tris Plus 10-well gels (Invitrogen, #MW04120BOX). Proteins were transferred to LF-PVDF membranes (BioRad, Hercules, CA, USA, #10026934) activated in 100% methanol. Following transfer, membranes were reactivated in 100% methanol.

Primary antibodies were diluted 1:1000 in 5% nonfat milk or 5% BSA dissolved in 1X TBS + 1% Tween-20 (TBST) as per the manufacturer protocol. Secondary antibodies were diluted 1:3333 in 5% nonfat milk dissolved in 1X TBST. Membranes were blocked for 1 h at room temperature in 5% nonfat milk or 5% BSA dissolved in 1X TBST, as per the manufacturer's protocol, followed by incubation with the primary antibodies on a rocker overnight at 4 °C. Membranes were washed three times in 1X TBST and incubated with the appropriate secondary antibody for 1 h at room temperature. For detection, the membranes were incubated in Clarity Western ECL Substrate (BioRad, #170-5061) or SuperSignal West Femto Maximum Sensitivity Substrate (BioRad, #34096) and

visualized with chemiluminescence using the BioRad ChemiDoc MP imaging system. Protein quantification was performed using Image Lab 6.0.1 software.

2.8. Sphingolipid Profiling

Lipids were extracted from cell homogenates equivalent to 400 mg of protein using a mix of isopropanol:water:ethyl acetate (3:1:6; *v:v:v*). Internal standards (10 pmol of d17 long-chain bases and C12 acylated sphingolipids) were added to samples at the onset of the extraction procedure. Extracts were separated on a Waters I-class Acquity UPLC chromatography system. Mobile phases were (A) 60:40 water:acetonitrile and (B) 90:10 isopropanol:methanol with both mobile phases containing 5 mM ammonium formate and 0.1% formic acid. A Waters C18 CSH 2.1 mm ID × 10 cm column maintained at 65 °C was used for the separation of the sphingoid bases, 1-phosphates, and acylated sphingolipids. The eluate was analyzed with an inline Waters TQ-S mass spectrometer using multiple reaction monitoring.

2.9. Cell Line Viability Assays

A total of 20,000 cells were seeded onto 96-well assay plates (Corning, #353072). LCL-805 was prepared by creating a 1:10 working stock in 37 °C RPMI-1640 supplemented with 10% FBS. Cells were treated with vehicle (DMSO) or LCL-805 at the indicated concentrations in a final volume of 100 µL and incubated for the indicated times. Following incubation, 20 µL of [3-(4,5-dimethylthiazol-2-yl)-5-(3-carboxymethoxyphenyl)-2-(4-sulfophenyl)-2H-tetrazolium] (MTS) (Promega, Madison, WI, USA, #G3582) was added and incubated at 37 °C for 3 h. Absorbance of the MTS-derived formazan product was measured at 490 nm with the Synergy HT plate reader (Biotek, Winooski, VT, USA). Following background subtraction, absorbances were normalized to vehicle control, which was defined as 100%. EC50 values were calculated with GraphPad Prism v9.5.1 using the function “log(inhibitor) vs. normalized response—variable slope”.

2.10. Patient Sample Viability Assays

In total, 5000 cells/well were seeded onto 384-well plates (ThermoFisher, #165195) and treated with vehicle (DMSO), LCL-805, CNL, or a combination for 48 h at the indicated concentrations. Viability was determined using the CellTiter-Glo luminescence assay (Promega, #G755B). Luminescence was measured using the GloMax Discover (Promega) as per the manufacturer’s protocol. Background media luminescence was subtracted from all samples, and luminescence data from drug-treated conditions were normalized to DMSO vehicle, which was set to 100%. EC50 values were determined as in Section 2.9.

2.11. Inhibitor Rescue Studies

For inhibitor rescue studies, cells were pretreated with vehicle (DMSO) or the indicated compounds for 2 h. Effective drug concentrations for rescue inhibitors were based on our prior publications [25,26]. We utilized rescue inhibitor concentrations at above and below these published concentrations and observed similar effects for each concentration. Following preincubation, cells were utilized for MTS viability studies, immunoblotting, or flow cytometry, as described in Section 2.9, Section 2.7, and Section 2.12, respectively.

2.12. Flow Cytometry

In total, 2.5×10^6 cells were seeded at a density of 2.5×10^5 cells/mL. LCL-805 was prepared by creating a 1:10 working stock in 37 °C RPMI-1640 supplemented with 10% FBS. Cells were treated with vehicle (DMSO) or LCL-805 at the indicated concentrations and incubated for the indicated times. Following treatment, cell death and mitochondrial membrane potential were evaluated using Muse Annexin V & Dead Cell Kit (Cytek, #MCH100105) and Muse MitoPotential Kit (Cytek, #MCH100110) per the manufacturer’s protocol. For each assay, the final cell dilutions were 1:4 and 500–2000 events were captured.

2.13. Synergy Analysis

Two-drug synergy was quantified using the online SynergyFinder 2.0 software [27]. The following parameters were used during analysis: Readout = Viability; Detect Outliers = Yes; Curve Fitting = LL4. Synergy scores represent the percentage differences between observed responses versus predicted responses calculated using the Bliss reference model. Scores above 10, between 10 and -10 , and below -10 are considered synergistic, additive, and antagonistic, respectively.

2.14. Statistical Analysis

Indicated statistical tests were performed using GraphPad Prism version 10.0.2. Results presented are representative data of at least two independent experiments. Each experiment contained at least three technical replicates. Error bars represent standard deviation.

3. Results

3.1. LCL-805 Inhibited AC in a Concentration- and Time-Dependent Manner

LCL-805 is an amino acid prodrug of B-13 and is structurally related to LCL-521 [22]. This class of prodrug traffics to lysosomes via its amino acid moiety where they are metabolized into the active ceramidase inhibitor B-13 [22]. We utilized a fluorescence-based assay to evaluate the effect of LCL-805 on AC activity [28]. Treatment of human AML cell lines MM-6 and OCI-AML2 with LCL-805 significantly reduced AC enzymatic activity in a concentration- and time-dependent manner (Figure 1A,B). Detection of the 13 kDa α -AC subunit is frequently used as a marker of active AC enzyme [29]. Consistent with the results of our activity assays, LCL-805 reduced the levels of the 13 kDa AC subunit in MM-6 and OCI-AML2 cells in a time-dependent manner (Figure 1C). Both readouts showed transient AC inhibition within 2 h post LCL-805 treatment. Together, these results demonstrated the AC inhibitory effects of LCL-805.

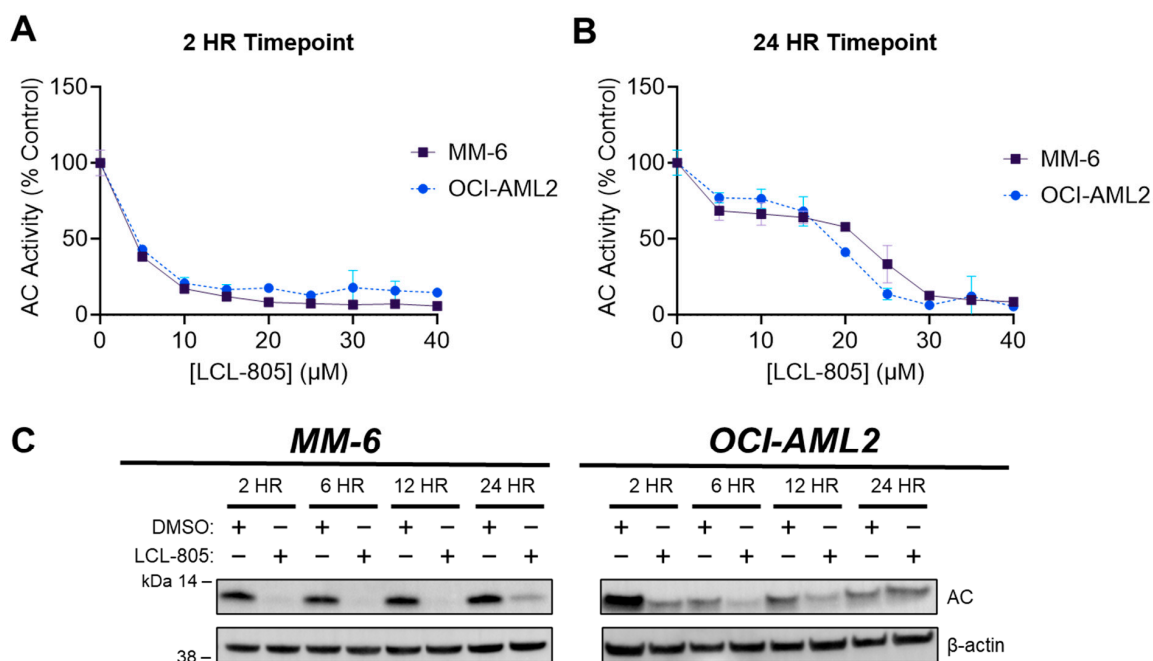


Figure 1. LCL-805 inhibited AC in a concentration- and time-dependent manner. (A,B) Fluorogenic AC activity assay conducted in MM-6 and OCI-AML2 human AML cell lines. Cells were treated with vehicle (DMSO) or the indicated concentration of LCL-805 for the indicated times. Error bars represent \pm standard deviation. (C) Immunoblotting of AC protein levels (α -subunit) in MM-6 and OCI-AML2 cells treated with DMSO or LCL-805 (15 μ M) for the indicated times. Data presented are representative experiments with at least three technical replicates. Whole, unedited western blot figures can be found in the supplementary materials.

3.2. LCL-805 Increased Cellular Ceramide and Decreased Sphingosine Levels

We next measured the effect of LCL-805 on sphingolipid content at these same time-points. AC is part of the sphingolipid metabolism “salvage pathway” and catabolizes ceramides into sphingosine and fatty acids. Upon AC inhibition, ceramides are expected to increase while sphingosine levels concurrently decrease. Indeed, sphingosine levels decreased substantially after 2 and 6 h of LCL-805 treatment in MM-6 and OCI-AML2 cells (Figure 2A,B). Sphingosine-1-phosphate (S1P) levels were minimally changed (Figure S1). Total ceramides were significantly elevated, with the greatest increase observed in OCI-AML2 cells (Figure 2C,D). Long-chain ceramides, such as C16-ceramide, may be more cytotoxic than very-long-chain ceramides, such as C24:1-ceramide [30]. We previously demonstrated that elevated C16-/C24:1-ceramide ratios are associated with increased cell death [11]. LCL-805 increased both C16- and C24:1-ceramides (Figure 2E,F) and C16-/C24:1-ceramide ratios (Figure 2G,H). Similar findings were observed for the C16-/C24-ceramide ratio (Figure S2). Ceramide elevation and sphingosine depletion were rapid but diminished over time. Levels of all ceramide species are shown in Figure S3 as well as comprehensive profiling of additional ceramide metabolites (Figures S4–S6). In summary, dihydroceramides were increased following LCL-805 treatment in both cell lines (Figure S4). Some hexosylceramides were increased (Figure S5), while sphingomyelin levels were mostly unchanged following LCL-805 treatment (Figure S6). Taken together, these results supported the AC inhibitory effects of LCL-805 which resulted in increased ceramides at the expense of sphingosine.

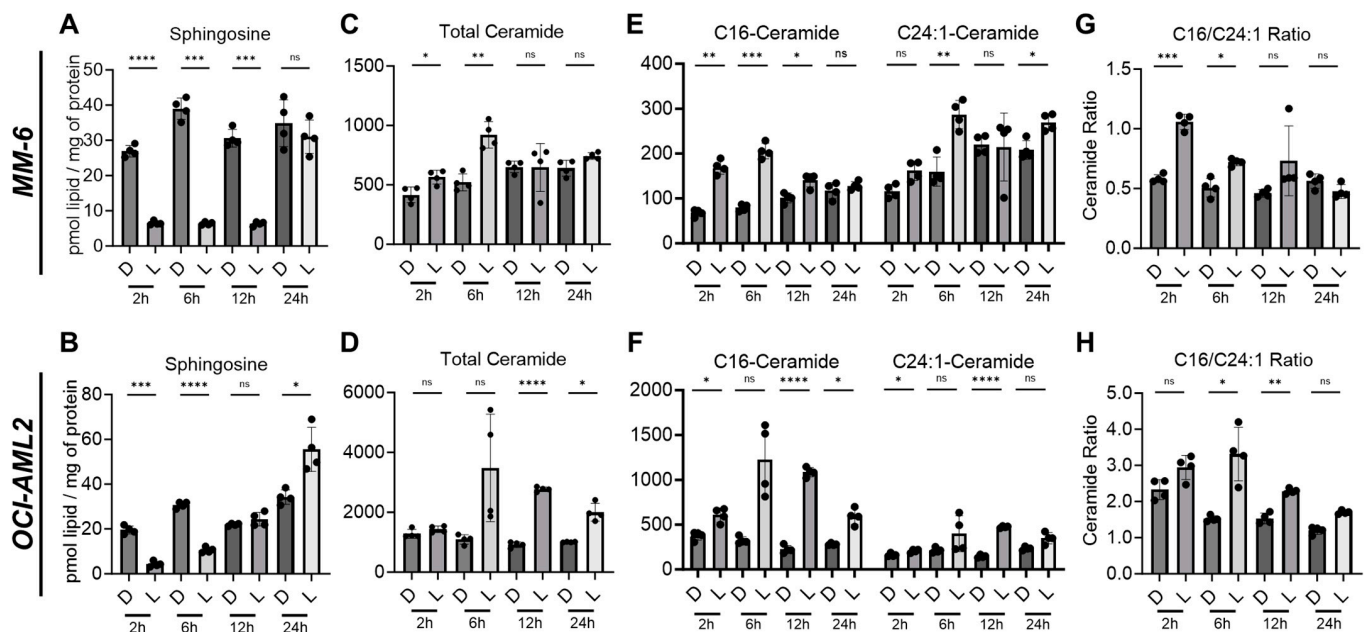


Figure 2. LCL-805 increased cellular ceramide and decreased sphingosine levels. Sphingolipid profiling of MM-6 and OCI-AML2 cells treated with vehicle (DMSO) or LCL-805 (15 μ M) for the indicated times. Levels of sphingosine (A,B), total ceramides (C,D), C16- and C24:1-ceramides (E,F), and C16-/C24:1-ceramide ratios (G,H) were evaluated with liquid chromatography–mass spectrometry. Bars represent the average of four technical replicates from a representative experiment. Error bars represent \pm standard deviation. Statistical analyses represent Welch’s ANOVA with Dunnett’s T3 multiple comparisons test. * $p < 0.05$, ** $p < 0.005$, *** $p < 0.001$, **** $p < 0.0001$, ns = non-significant. D = DMSO; L = LCL-805. C## = fatty acid chain length. Total = sum of sphingolipid species.

3.3. LCL-805-Induced Loss of AML Cell Viability Is Characterized by Increased Phosphatidylserine Externalization and Mitochondrial Depolarization

We next evaluated LCL-805 effects on cell viability across 32 human AML cell lines. A median EC₅₀ of 11.7 μ M was achieved across these cell lines (Figure 3A,B). We also utilized several parental/drug-resistant cell line pairs and showed that LCL-805 was equipotent in drug-resistant cell lines (Figure 3B). LCL-805 was then evaluated as a single agent across a panel of primary AML patient samples. LCL-805 demonstrated efficacy (median EC₅₀ value of 15.8 μ M) in 52.9% of the patient samples. The remaining 47.1% of the samples were resistant to the maximal concentration tested of 20 μ M (Figure 3C).

We next utilized flow cytometry to measure phosphatidylserine externalization (annexin V staining) and 7-aminoactinomycin D (7-AAD staining). We observed a significant concentration-dependent increase in single annexin V-positive, single 7-AAD-positive, and double-positive cells following LCL-805 treatment (Figure 4A,B). As AC inhibition is deleterious to mitochondrial function in AML [31] and pancreatic cancer [32], we investigated the effects of LCL-805 on mitochondrial membrane potential. In MM-6 and OCI-AML2 cells, LCL-805 treatment promoted concentration-dependent mitochondrial depolarization (Figure 4C,D). Representative flow cytometry plots are provided in Supplemental Figure S7. Taken together, these findings demonstrated that LCL-805 reduced cell viability, induced phosphatidylserine externalization, and triggered mitochondrial membrane depolarization within the micromolar range.

3.4. Inhibition of Caspases, Lysosomal Cathepsins, Autophagy, or Necroptosis Did Not Protect against LCL-805 Cytotoxicity

Previous reports of B-13 analog cell death mechanisms are divergent, with some indicating caspase-dependent apoptosis [12] and others indicating caspase-independent non-apoptotic cell death [33]. To determine whether caspase-3 is activated following LCL-805 treatment, we treated AML cells with LCL-805 and measured caspase-3 cleavage via immunoblotting. We detected partial cleaved caspase-3 in MM-6 which increased over time. Weaker cleaved caspase-3 was detected in OCI-AML2 cells (Figure 5A,B). Poly (ADP-ribose) polymerase-1 (PARP) cleavage is routinely used as a marker of caspase activation and was observed at 12 h and 24 h post LCL-805 treatment, with weaker cleavage detected in OCI-AML2 cells (Figure 5A,B). Sphingolipids are linked to Bcl-2 family proteins, gatekeepers of caspase-dependent apoptotic cell death [14], and the endogenous caspase inhibitor, X-linked inhibitor of apoptosis protein (XIAP) [34,35]. LCL-805 treatment did not decrease the protein levels of the anti-apoptotic proteins Mcl-1, Bcl-2, Bcl-xL, or XIAP (Figure 5A,B). Pretreatment with the pan-caspase inhibitor zVAD-FMK did not protect MM-6 or OCI-AML2 cells from LCL-805 cytotoxicity (Figure 6A,B). As other iterations of B-13 analogs destabilize lysosomes [36] or induce cell death via lysosomal cathepsin activity [33], we also evaluated the contribution of lysosomal cathepsins in LCL-805 killing. Pretreating cells with CA-074me or pepstatin-A, cathepsin B and D inhibitors, respectively, did not protect against LCL-805 killing (Figure S8A,B). These findings show that caspases or lysosomal cathepsins were not the primary mediators of LCL-805 cytotoxicity.

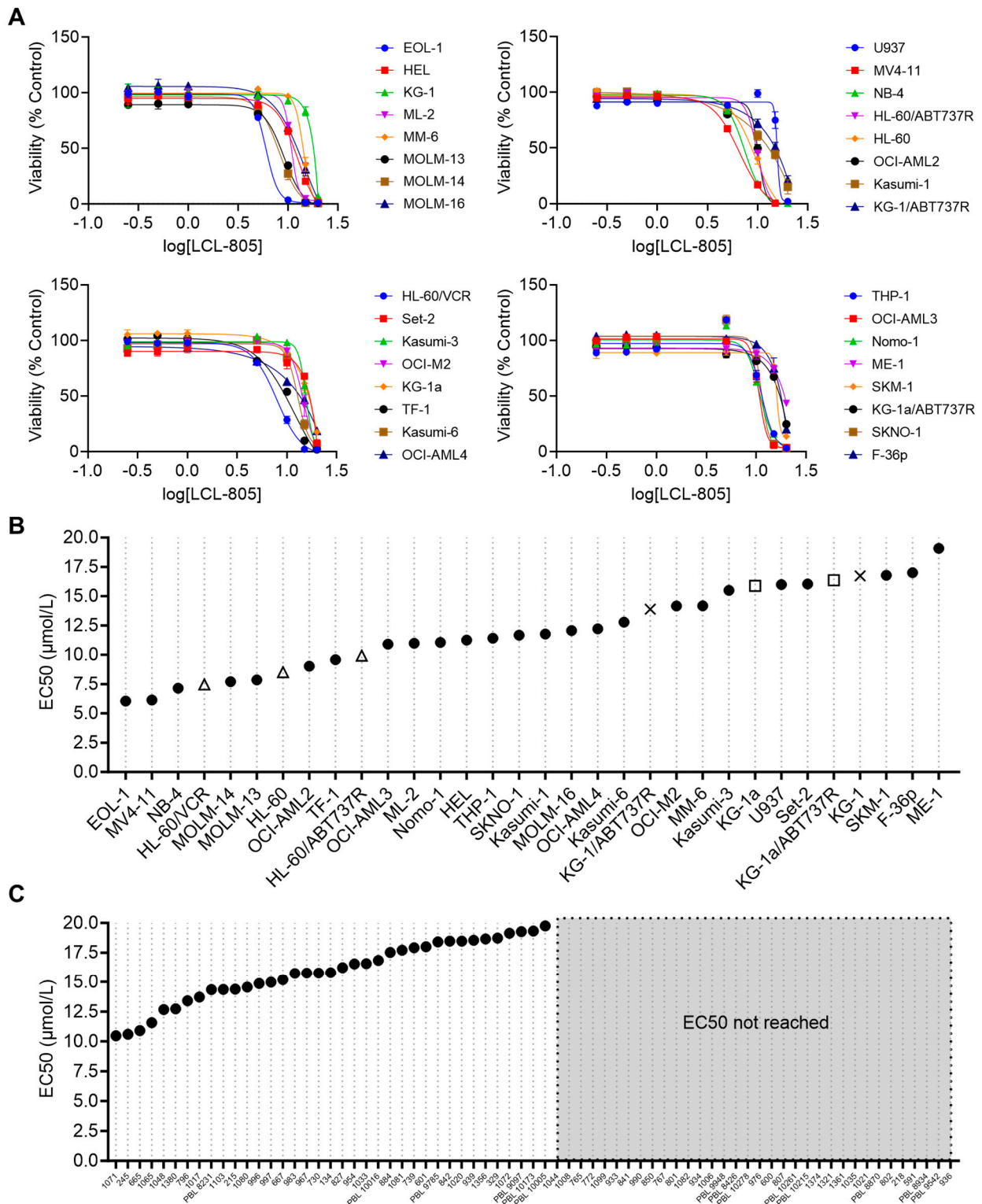


Figure 3. LCL-805 reduced viability of human AML cell lines and primary patient samples. (A) Cell viability of 32 human AML cell lines treated with vehicle (DMSO) or the indicated concentrations of LCL-805 for 48 h. (B,C) Calculated LCL-805 EC50 values across AML cell lines (B) or primary AML patient samples (C). Legend for parental and drug-resistant cell line pairs: HL-60 (Δ); KG-1 (\times); KG-1a (\square); ABT737R = ABT737-resistant; VCR = vincristine-resistant. Data represent the average of three technical replicates from a representative experiment. Error bars represent +/− standard deviation.

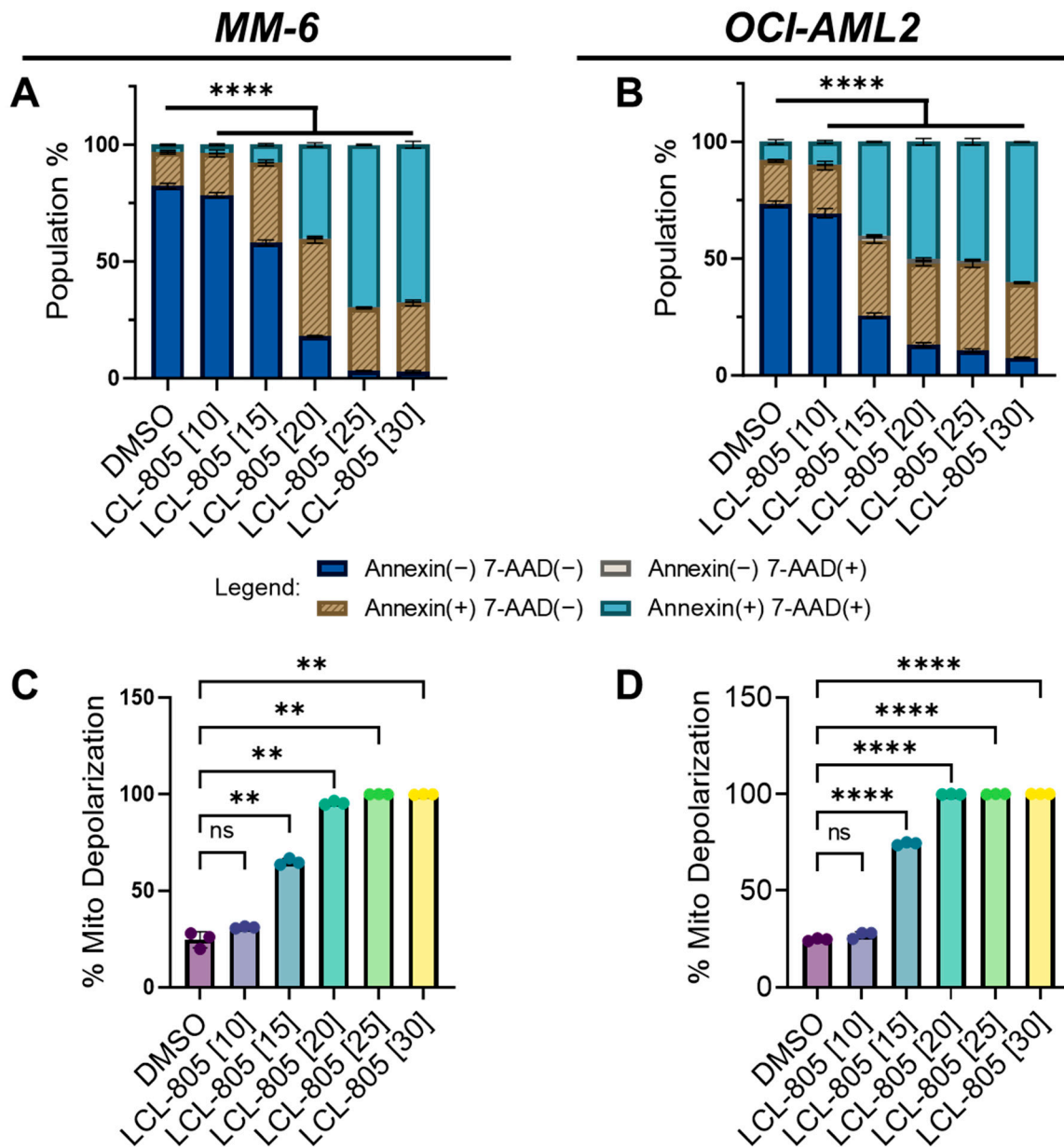


Figure 4. LCL-805 increased phosphatidylserine externalization and triggered mitochondrial depolarization. (A,B) Annexin V and 7-AAD flow cytometry in MM-6 and OCI-AML2 treated for 24 h with vehicle (DMSO) or the indicated concentrations of LCL-805 (in μM , shown in brackets). (C,D) Mitochondrial membrane potential in MM-6 and OCI-AML2 treated for 24 h with DMSO or the indicated concentrations of LCL-805. Bars represent the average of three technical replicates from a representative experiment. Error bars represent \pm standard deviation. Statistical analyses represent two-way ANOVA with Dunnett's multiple comparisons test (A,B) and Welch's ANOVA with Dunnett's multiple comparisons test (C,D). ** $p < 0.005$, **** $p < 0.0001$, ns = non-significant.

We next evaluated whether autophagy was involved in LCL-805-mediated cell death. Microtubule-associated protein light chain 3 (LC3) is a key component of autophagosome formation, and its processing from LC3-I to LC3-II is commonly used to measure autophagosome formation and autophagic flux [37]. Increased LC3A-II protein levels after LCL-805 treatment suggested increased autophagosome formation or decreased autophagic flux (Figure 5A,B). We leveraged pharmacological and genetic autophagy inhibition to evaluate the role of autophagy in LCL-805-mediated killing. Chloroquine and bafilomycin A1 are late-stage autophagy inhibitors that antagonize autophagosome fusion with the

lysosome [38] and disrupt the acidification of the autolysosome [39]. Pretreatment with chloroquine (Figure 6C,D) or bafilomycin A1 (Figure 6E,F) did not protect against but rather slightly enhanced LCL-805 toxicity. Autophagy-Related 5 (ATG5) and Autophagy-Related 7 (ATG7) are critical for autophagosome formation and LC3 processing [37]. To determine how depleting autophagy machinery affects LCL-805 killing, we evaluated LCL-805 toxicity in MV4-11 human AML cells deficient in ATG5 or ATG7 previously generated by our group [25]. Neither ATG5 nor ATG7 knockout affected AC protein levels (Figure 6G). Consistent with our pharmacological inhibition studies, the knockout of ATG5 or ATG7 did not blunt LCL-805 cytotoxicity (Figure 6H). We next evaluated whether necroptotic cell death was involved in LCL-805 killing. Ceramides have previously been implicated in necroptosis, a form of regulated cell death that involves the activation of receptor-interacting protein kinase 1 (RIPK1) and receptor-interacting protein kinase 3 (RIPK3) [40,41]. Pretreating AML cells with the RIPK1 inhibitor necrostatin-1 or the RIPK3 inhibitor GSK'872 did not protect against LCL-805 cytotoxicity (Figure S8C). Taken together, these findings suggested that autophagy and RIPK1/3 activation were not the primary mediators of LCL-805 cytotoxicity.

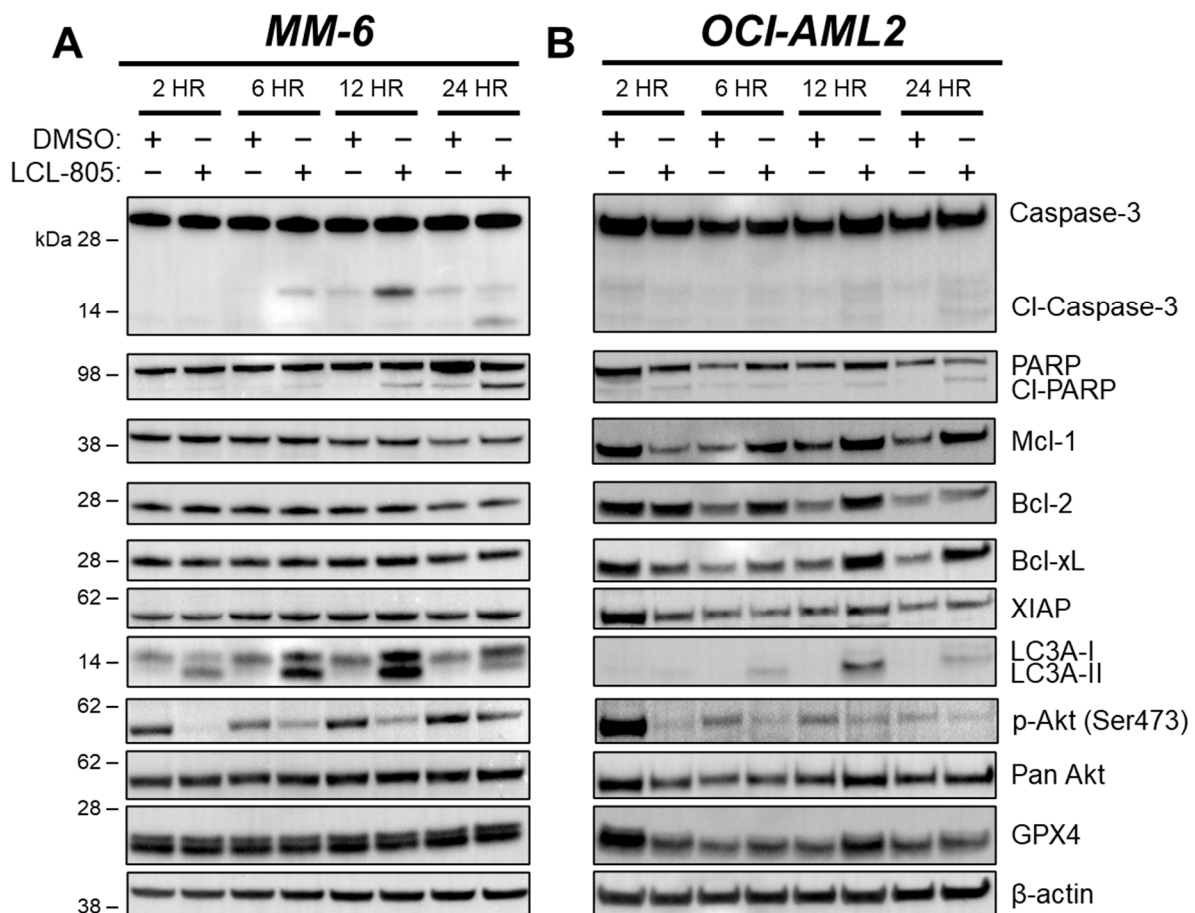


Figure 5. LCL-805 induced caspase-3 and PARP cleavage, LC3A processing, and reduced Akt phosphorylation. Immunoblotting of MM-6 (A) and OCI-AML2 cells (B) treated with DMSO or LCL-805 (15 μ M) for the indicated times. Data are from a representative experiment. Whole, unedited western blot figures can be found in the supplementary materials.

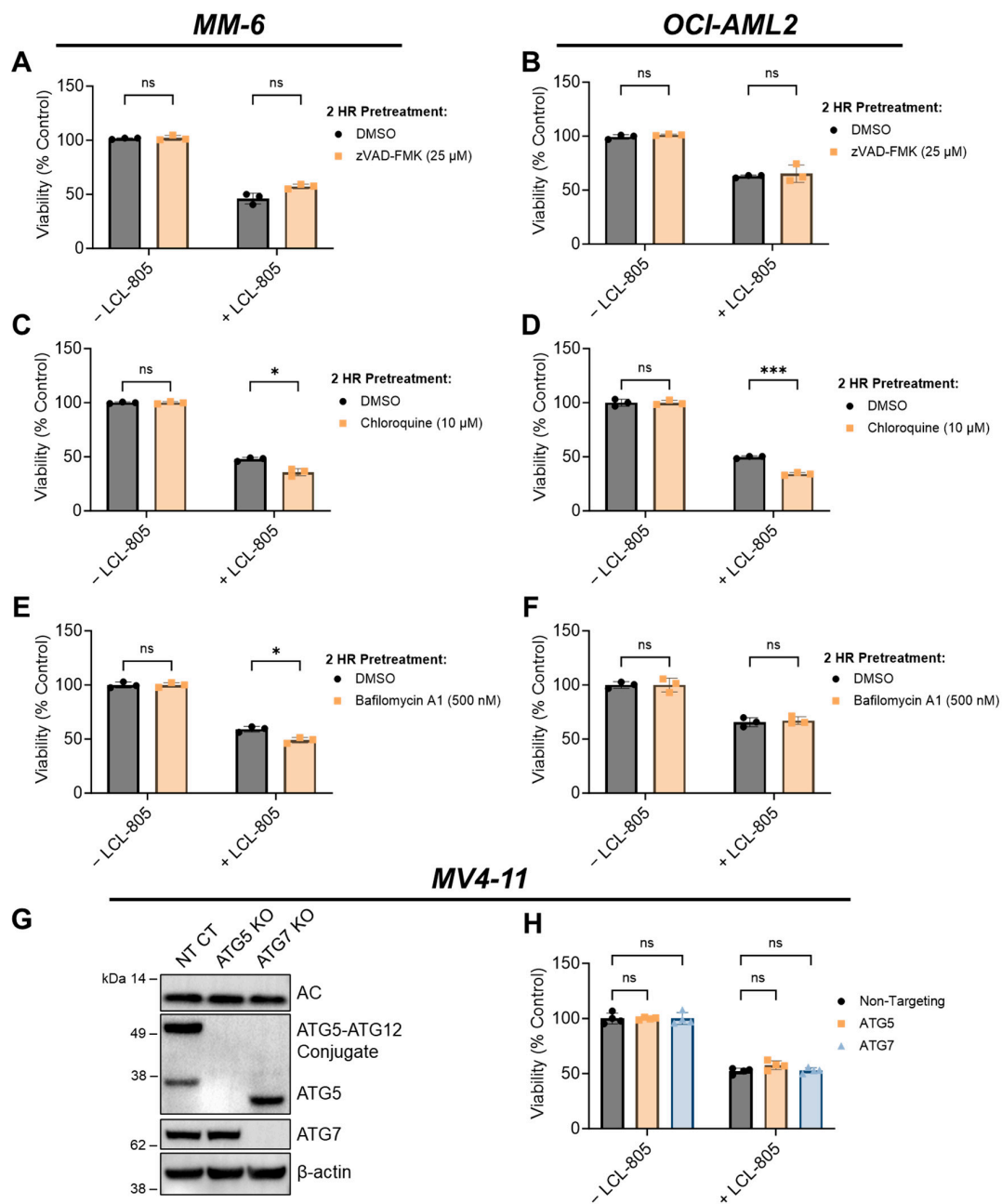


Figure 6. Inhibition of caspases or autophagy did not rescue LCL-805-mediated cell death. (A,B) Cell viability of MM-6 and OCI-AML2 cells pretreated with vehicle (DMSO) or zVAD-FMK (25 μ M) for 2 h and subsequently treated with DMSO or LCL-805 (15 μ M) for 24 h. (C,D) Cell viability of MM-6 and OCI-AML2 cells pretreated with vehicle (DMSO) or chloroquine (10 μ M) for 2 h and subsequently treated with DMSO or LCL-805 (C = 20 μ M; D = 17.5 μ M) for 24 h. (E,F) Cell viability of MM-6 and OCI-AML2 cells pretreated with vehicle (DMSO) or bafilomycin A1 (500 nM) for 2 h and subsequently treated with DMSO or LCL-805 (E = 20 μ M; F = 17.5 μ M) for 24 h. (G) Immunoblotting of AC (α -subunit), ATG5, and ATG7 protein levels in non-targeting control (NT CT), ATG5-deficient (ATG5 KO), or ATG7-deficient (ATG7 KO) MV4-11 cells. (H) Cell viability of NT CT, ATG5 KO, or ATG7 KO MV4-11 cells treated with vehicle (DMSO) or LCL-805 (10 μ M) for 24 h. Bars represent the average of three technical replicates from a representative experiment. Error bars represent \pm standard deviation. Statistical analyses represent unpaired Welch's *t*-tests with Holm-Šidák's multiple comparisons test (A–F) and two-way ANOVA with Dunnett's multiple comparisons test (H). * $p < 0.05$, *** $p < 0.001$, ns = non-significant. Whole, unedited western blot figures can be found in the supplementary materials.

3.5. Akt Reactivation and Iron Chelation Rescued LCL-805-Induced Cell Death

Aberrant Akt signaling, as evidenced by high levels of phospho-Akt, is a therapeutically relevant AML hallmark [42–44]. Moreover, AC activity is associated with oncogenic Akt signaling [45,46], which prompted us to evaluate the effects of LCL-805 on Akt. Akt phosphorylation at Ser473 and Thr308 contributes to its full activity. LCL-805 treatment significantly reduced Ser473 phosphorylation in MM-6 and OCI-AML2 cells (Figure 5A,B). To assess whether Akt antagonism mediated LCL-805 cytotoxicity, we measured cell viability in cells pretreated with the Akt activator SC-79, which binds Akt and promotes an active conformation [47], then treated with LCL-805. SC-79 pretreatment protected against LCL-805-induced loss of cell viability in both MM-6 and OCI-AML2 cells (Figure 7A,B). In MM-6 cells, SC-79 pretreatment increased Ser473 Akt phosphorylation following 24 h LCL-805 treatment. In OCI-AML2 cells, we observed weaker increases in Ser473 phosphorylation (Figure 7C). Together, these findings demonstrated that Akt inhibition contributed to LCL-805 toxicity, and pharmacological Akt reactivation protected against LCL-805 cytotoxicity.

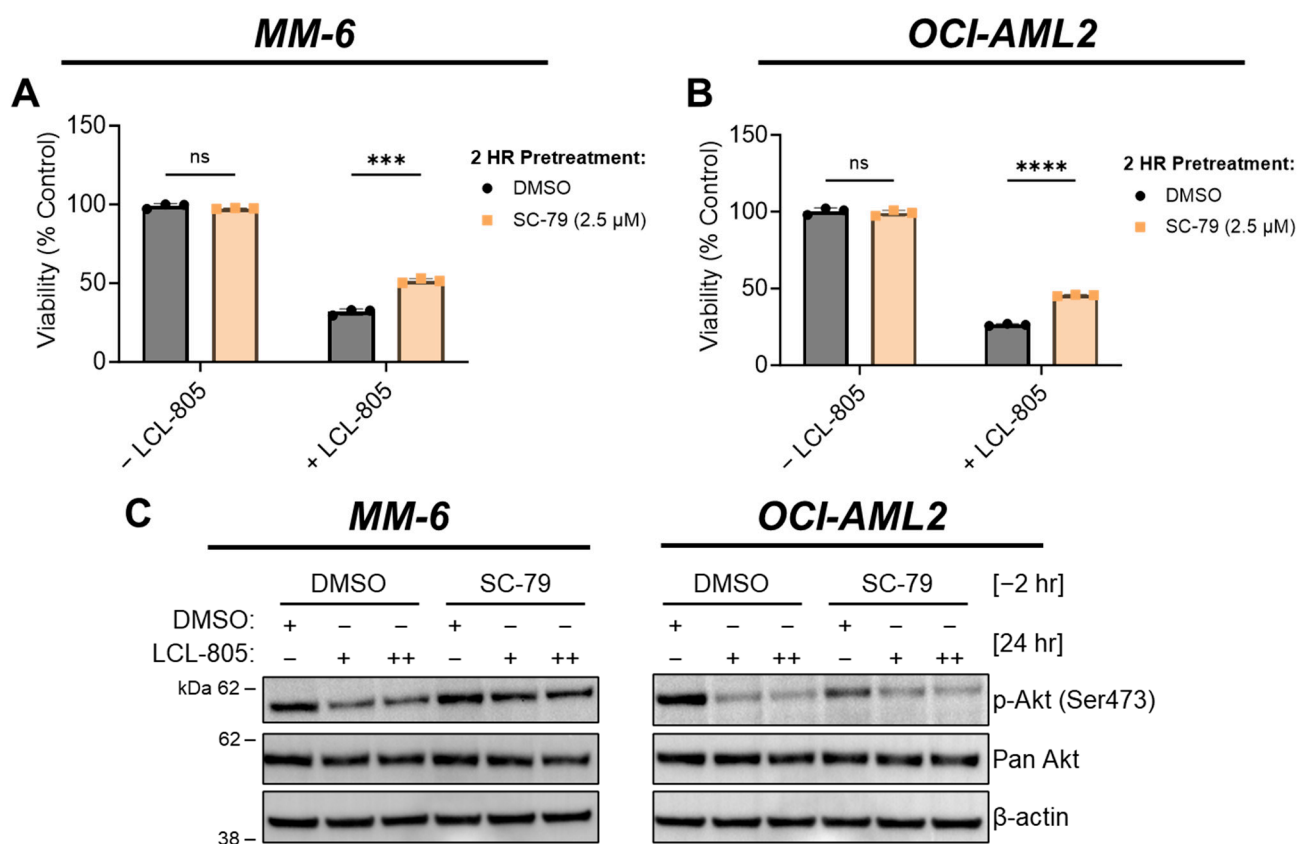


Figure 7. Akt reactivation rescued LCL-805-induced cell death. (A,B) Cell viability of MM-6 and OCI-AML2 cells pretreated with vehicle (DMSO) or SC-79 (2.5 μM) for 2 h and subsequently treated with DMSO or LCL-805 (A = 20 μM; B = 17.5 μM) for 24 h. (C) Immunoblotting of MM-6 and OCI-AML2 cells pretreated with SC-79 (2.5 μM) for 2 h then treated with DMSO or LCL-805 (MM-6: + = 17.5 μM, ++ = 20 μM; OCI-AML2: + = 12.5 μM, ++ = 15 μM) for 24 h. Bars represent the average of three technical replicates from a representative experiment. Error bars represent +/− standard deviation. Statistical analyses represent unpaired Welch’s *t*-tests and Holm–Šidák’s multiple comparisons test. *** $p < 0.001$, **** $p < 0.0001$, ns = non-significant. Whole, unedited western blot figures can be found in the supplementary materials.

As an extension of their role as cellular recycling centers, lysosomes are critical regulators of iron trafficking, storage, and metabolism [48]. Deferoxamine mesylate (DFO) is an FDA-approved iron-chelating agent used to treat acute iron intoxication and chronic iron

overload. We tested the effects of iron chelation on LCL-805 toxicity and found that DFO pretreatment significantly protected AML cells from LCL-805 cytotoxicity (Figure 8A,B). Because iron is necessary for ferroptotic cell death, which is characterized by iron accumulation and lipid peroxidation, we evaluated whether pharmacological ferroptosis inhibitors rescued LCL-805 killing. Treatment with the ferroptosis inhibitors liproxstatin-1 (Figure 8C,D) or ferrostatin-1 (Figure 8E,F) did not attenuate LCL-805-mediated cell death. Moreover, LCL-805 treatment did not affect protein levels of glutathione peroxidase 4 (GPX4), a master regulator of canonical ferroptosis (Figure 5A,B). To determine how DFO protected against LCL-805 cytotoxicity, we evaluated protein changes in LCL-805-treated AML cells with or without DFO pretreatment (Figure 8G). GPX4 protein levels and Akt phosphorylation were unchanged following LCL-805 with or without DFO pretreatment. DFO is a known HIF-1 α activator [49]. While treatment with DFO alone increased HIF-1 α protein levels in MM-6 cells, DFO and LCL-805 treatment synergistically stabilized HIF-1 α protein expression, suggesting a protective role for HIF-1 α in LCL-805 cytotoxicity. Taken together, these findings demonstrated that LCL-805 antagonized Akt signaling and induced iron-dependent cell death distinct from canonical ferroptosis.

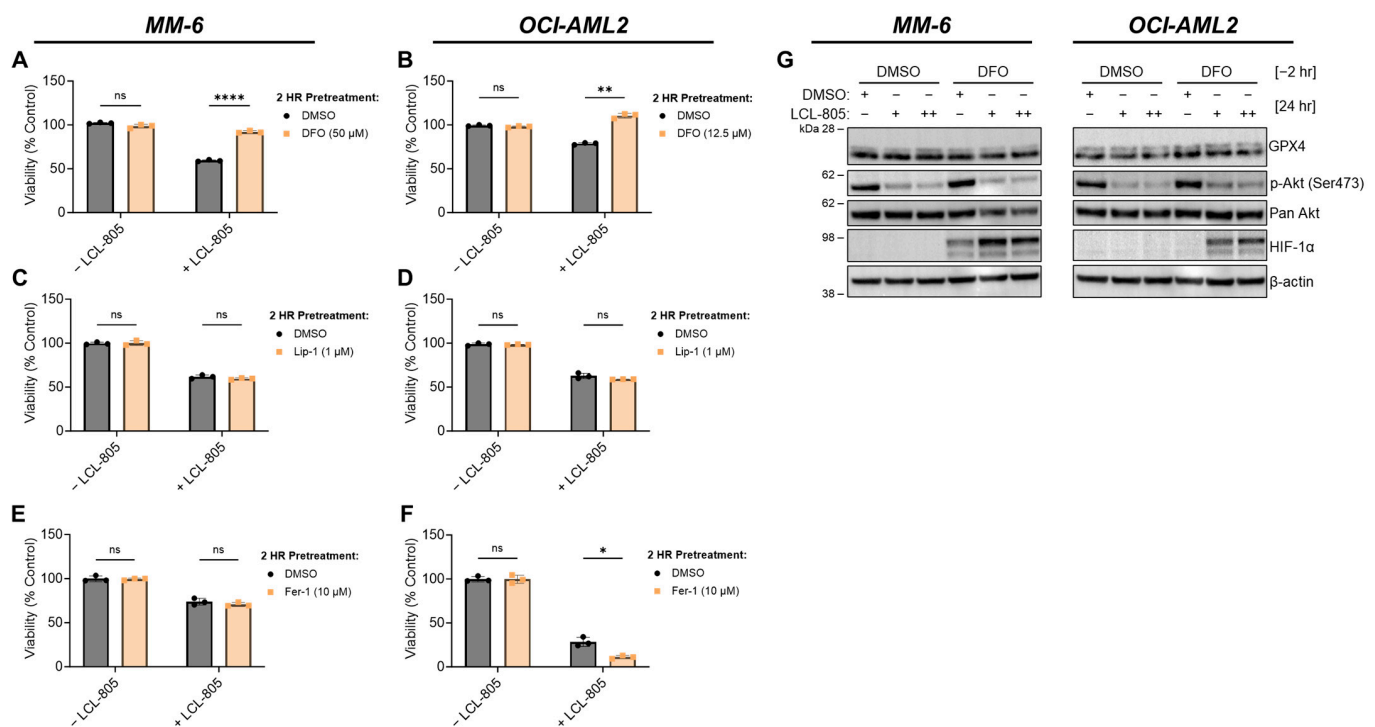


Figure 8. Iron chelation rescued LCL-805-induced cell death. (A,B) Cell viability of MM-6 and OCI-AML2 cells pretreated with vehicle (DMSO) or the indicated concentration of DFO for 2 h and subsequently treated with DMSO or LCL-805 (15 μ M) for 24 h. (C,D) Cell viability of MM-6 and OCI-AML2 cells pretreated with vehicle (DMSO) or the indicated concentration of liproxstatin-1 (Lip-1) for 2 h and subsequently treated with DMSO or LCL-805 (C = 20 μ M; D = 17.5 μ M) for 24 h. (E,F) Cell viability of MM-6 and OCI-AML2 cells pretreated with vehicle (DMSO) or the indicated concentration of ferrostatin-1 (Fer-1) for 2 h and subsequently treated with DMSO or LCL-805 (E = 15 μ M; F = 15 μ M) for 24 h. (G) Immunoblotting of MM-6 and OCI-AML2 cells pretreated with DFO for 2 h (DFO; MM-6 = 50 μ M; OCI-AML2 = 12.5 μ M) then treated with DMSO or LCL-805 (MM-6: + = 15 μ M, ++ = 17.5 μ M; OCI-AML2: + = 12.5 μ M, ++ = 15 μ M) for 24 h. Bars represent the average of three technical replicates from a representative experiment. Error bars represent +/− standard deviation. Statistical analyses represent unpaired Welch’s *t*-tests and Holm–Šidák’s multiple comparisons test. * $p < 0.05$, ** $p < 0.005$, **** $p < 0.0001$, ns = non-significant. Whole, unedited western blot figures can be found in the supplementary materials.

3.6. C6-Ceramide Nanoliposome (CNL) Supplementation Improved LCL-805 Toxicity

LCL-805 increased pro-death ceramides and the C16-/C24:1- and C16-/C24-ceramide ratios, which prompted us to evaluate the cytotoxic effects of combining exogenous ceramide with LCL-805. To this end, we tested LCL-805 and CNL across a panel of primary AML patient samples. The effect of LCL-805, CNL, or the combination on cell viability and the corresponding Bliss synergy scores from the top five patient samples most sensitive to the combination are shown in Figure 9A,B. LCL-805 and CNL demonstrated modest efficacy as single agents. However, the combination resulted in highly potent synergistic lethality (Figure 9A,B). Treatment of AML patient samples with the CNL and LCL-805 combination demonstrated synergistic ($n = 48$) or additive ($n = 16$) Bliss synergy scores, while only one exhibited antagonism (Figure 9C). We also compared these results in primary AML patient samples to nine healthy donor normal samples (seven PBMC and two whole bone marrow samples). As single agents, LCL-805 and CNL demonstrated similar loss of viability in primary AML patient samples and normal controls. The combination of LCL-805 and CNL reduced cell viability more in leukemic AML patient samples compared to healthy donor samples although the differences were not statistically significant (Figure 9D). Cell viability dropped to less than 50% in only 52.9% of patient samples treated with single-agent LCL-805 up to 20 μ M (Figure 3C). However, the addition of CNL (5 μ M) with 15 μ M LCL-805 resulted in a loss of cell viability greater than 50% in 70.8% of patient samples (Figure 9D). Together, these results demonstrate the promising therapeutic effects of combining AC inhibition with exogenous ceramide supplementation.

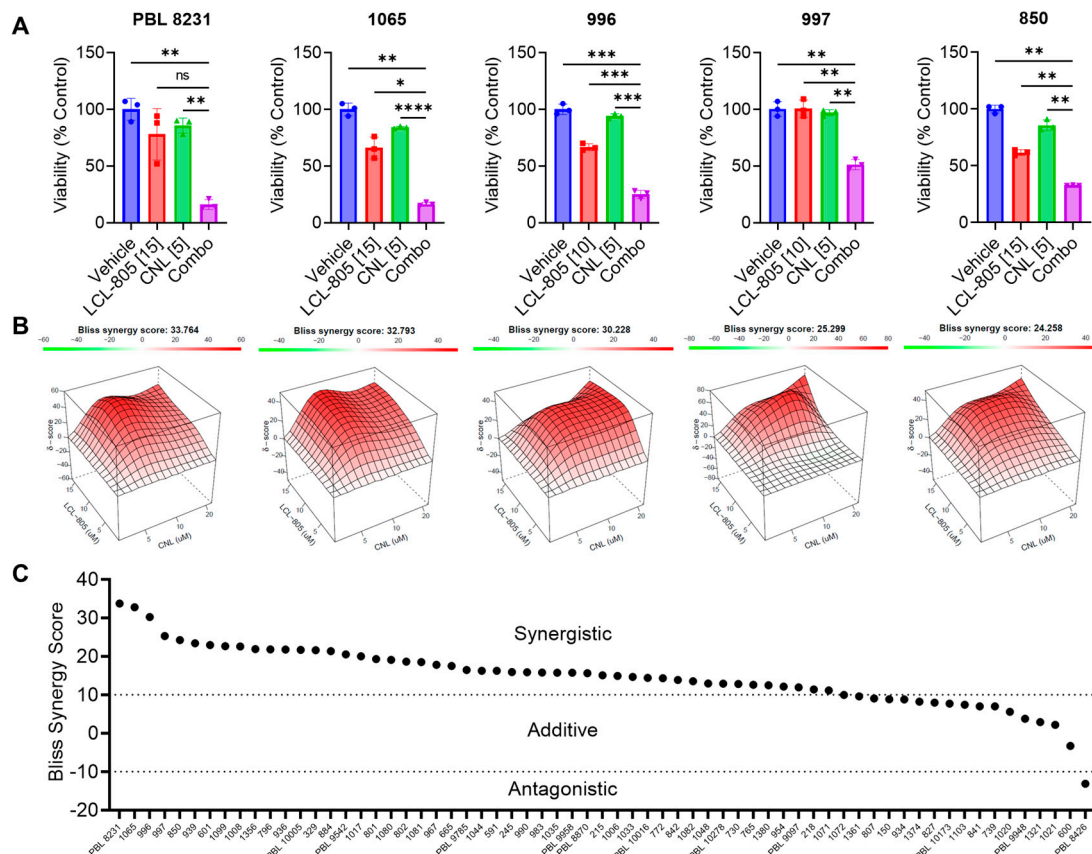


Figure 9. Cont.

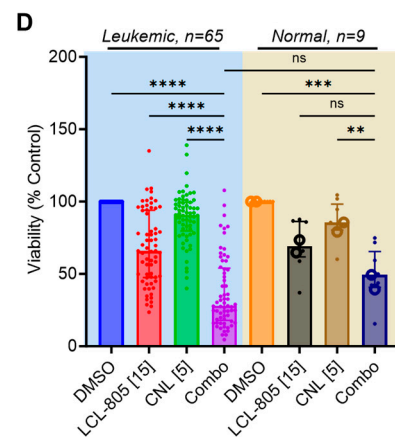


Figure 9. C6-ceramide nanoliposome (CNL) supplementation increased LCL-805 toxicity. Cell viability was measured in primary AML patient samples treated with multiple concentrations of LCL-805 (5, 10, or 15 μ M) and CNL (5, 10, or 20 μ M). (A) Cell viability and Bliss synergy scores (B) of the top five AML patient samples with the highest synergy scores treated with vehicle (DMSO), LCL-805, CNL, or the combination. Drug concentration (in μ M) is indicated in brackets within the x-axis labels. (C) Bliss synergy scores of primary AML patient samples treated with LCL-805 and CNL. (D) Cell viability of primary AML patient samples or normal controls (7 PBMC samples (●) and 2 CD34+ bone marrow samples (○)) treated with DMSO, LCL-805, CNL, or the combination. Drug concentration (in μ M) is indicated in brackets within the x-axis labels. Bars represent the average of three technical replicates from a representative experiment. Error bars represent \pm standard deviation. Statistical analyses represent Welch ANOVA with Dunnett's multiple comparisons test. * $p < 0.05$, ** $p < 0.005$, *** $p < 0.001$, **** $p < 0.0001$, ns = non-significant.

4. Discussion

AC is a lysosomal ceramide-catabolizing enzyme that is actively being explored as a therapeutic target in multiple solid and hematologic malignancies [18]. Our group showed that AC is overexpressed in AML, supports leukemic blast survival, and contributes to drug resistance [12,15]. In this work, we evaluated the anti-leukemic efficacy and cell death mechanisms of the dimethylglycine (DMG)-B-13 prodrug LCL-805 in AML. B-13 is a ceramide analog and ceramidase inhibitor with demonstrated anti-tumor properties [20,21]. The AC-targeting properties of B-13 were improved via the synthesis of lysosome-localizing DMG-B-13 prodrugs [22]. We showed that LCL-805 was an effective AC inhibitor and modulator of sphingolipid content with demonstrated anti-leukemic efficacy exacerbated by CNL supplementation *in vitro*. Our mechanistic studies showed that the cell death mechanisms of LCL-805 were not mediated through caspase-dependent apoptosis, lysosomal cathepsins, autophagy, or necroptosis. Instead, our findings revealed that LCL-805 toxicity was mediated by Akt antagonism and an iron-dependent form of cell death distinct from canonical ferroptosis.

LCL-805 is structurally related to another DMG-B13-prodrug, LCL-521. We compare our LCL-805 findings with published work evaluating the anticancer properties, sphingolipid modulating effects, and cell death mechanisms of LCL-521. LCL-521 has demonstrated anti-tumor efficacy and reduces sphingosine and S1P levels in cell line models of human breast adenocarcinoma [50]. A follow-up study evaluated the concentration-dependent effects of LCL-521 on AC protein levels and sphingolipid metabolites [51]. AC inactivation and decreased sphingosine content following LCL-521 treatment were reversible, which is consistent with our observed effects of LCL-805 on AC activation and sphingosine content in AML. Our observation of increased dihydroceramides following LCL-805 treatment is consistent with the finding that high concentrations of LCL-521 inhibit the enzyme responsible for converting dihydroceramides to ceramides, dihydroceramide desaturase-1 [51].

A separate study evaluated the mechanisms by which LCL-521 targeted myeloid-derived suppressor cells [33] and showed that LCL-521-mediated cytotoxicity was blunted by inhibiting cathepsins B and D. In contrast, loss of cell viability was not rescued following cathepsin inhibition in our studies. We instead showed that Akt activation and iron chelation protected against LCL-805 cytotoxicity. LCL-805-mediated cell death was not rescued by the ferroptosis inhibitors liproxstatin-1 or ferrostatin-1 despite the protective effect of iron chelation. Iron chelation with DFO stabilized HIF-1 α protein expression, which was further enhanced by LCL-805 treatment. HIF-1 α stabilization promotes drug resistance in multiple leukemias, suggesting that HIF-1 α stabilization protected against LCL-805 cytotoxicity [52]. These findings suggest that LCL-805 elicited a mode of iron-dependent cell death distinct from canonical ferroptosis. Differences in cell types evaluated between our study (human AML) versus the LCL-521 study (murine reticulum cell sarcoma) may contribute to the contrasting cell death mechanisms. Because lysosomes are a critical component of iron metabolism and AML cells are characterized by iron overload, the lysosome-targeting properties of LCL-805 may exacerbate an iron-dependent mode of cell death specific for AML [48,53].

Multiple studies demonstrate that ceramide accumulation or the addition of exogenous ceramides antagonizes Akt signaling [9]. In addition, others have linked AC to Akt-mediated cancer survival, drug resistance, and progression [45,46]. We observed strong basal levels of Akt phosphorylation at Ser473 in MM-6 and OCI-AML2 cells. LCL-805 treatment dramatically reduced Akt phosphorylation. Supplementation with the Akt activator SC-79 protected against LCL-805 toxicity, suggesting that Akt inactivation contributed to LCL-805 toxicity. In prostate cancer, AC overexpression promoted Akt activation involving sphingosine kinase 1 and S1P receptor 2 [46]. In our work, LCL-805-mediated S1P changes were modest, suggesting that the inhibitory effects of LCL-805 on Akt were likely mediated by elevated ceramide levels rather than loss of S1PR signaling.

The relationship between ceramide accumulation and cancer cell death provided the rationale to combine exogenous ceramide with LCL-805 to enhance ceramide accumulation in the context of AC blockade. Previously, solubility and delivery issues due to the lipophilic nature of ceramides hindered exogenous ceramide supplementation as a viable treatment option. However, this major hurdle was overcome in part by the development of C6-ceramide-containing nanoliposomes (CNLs) [10]. The LCL-805 and CNL combination resulted in potent synergistic lethality in primary AML patient samples, warranting additional preclinical studies to define the efficacy and synergistic mechanisms of this combination. CNL completed a phase I trial in advanced solid cancers [54] and is currently entering a phase I/II trial as a single agent and in combination with vinblastine or with venetoclax and low-dose Ara-C (LDAC) in relapsed/refractory AML. Sphingolipid metabolism and the regulation of mitochondrial apoptosis via Bcl-2 family proteins are intricately linked [55,56]. The specific Bcl-2 inhibitor venetoclax is approved for use in AML in combination with LDAC or hypomethylation agents. However, high relapse rates from venetoclax-containing regimens provide the rationale and impetus to develop more effective venetoclax-based drug combinations. Ceramide-generating therapeutics in the form of exogenous ceramide [11] and sphingosine kinase inhibitors [57] improve the efficacy of venetoclax-containing AML regimens. These data highlight the utility of future studies combining AC inhibition with venetoclax.

The *in vivo* anti-leukemic efficacy of LCL-805 remains elusive as it exhibited toxicity and poor pharmacokinetic features (Figure S9). Thus, it failed to show efficacy in pre-clinical human cell line xenograft studies (Figure S10). Future studies await improved nanoformulations or structural modifications of LCL-805 or its derivatives.

5. Conclusions

In summary, our key findings demonstrate that AC inhibition with LCL-805 promoted ceramide accumulation, Akt inactivation, and an iron-dependent mode of cell death. LCL-805 was toxic towards AML cell lines and primary patient samples and synergized with

C6-ceramide-containing nanoliposomes. Because of its role in maintaining AML survival, AC remains a promising therapeutic drug target, and further development of AC inhibitors is warranted.

Supplementary Materials: The following supporting information can be downloaded at <https://www.mdpi.com/article/10.3390/cancers15245866/s1>, Figure S1: Effect of LCL-805 on sphingosine-1-phosphate levels; Figure S2: LCL-805 increased the C16-/C24-ceramide ratio; Figure S3: Effect of LCL-805 on ceramide levels; Figure S4: Effect of LCL-805 on dihydroceramide levels; Figure S5: Effect of LCL-805 on hexosylceramide levels; Figure S6: Effect of LCL-805 on sphingomyelin levels; Figure S7: Flow cytometry-based detection of phosphatidylserine externalization and mitochondrial depolarization with LCL-805 treatment; Figure S8: Inhibiting lysosomal cathepsins or necroptosis did not rescue LCL-805-mediated cytotoxicity; Figure S9: LCL-805 pharmacokinetics; Figure S10: Lack of LCL-805 efficacy in an AML cell line-derived xenograft (CDX) mouse model; Whole, unedited western blot figures (Figures S11–S17); Table S1: AML patient sample cohort.

Author Contributions: Conceptualization, J.U., S.-F.T., C.E.C., M.C.C., D.J.F. and T.P.L.; methodology, T.E.F.; validation, J.U. and M.T.; formal analysis, J.U. and B.J.H.; investigation, J.U., J.J.P.S., M.T., U.G. and A.S.; resources, Z.M.S., H.-G.W. and D.F.C.; writing—original draft preparation, J.U., S.-F.T. and D.J.F.; writing—review and editing, all co-authors; supervision, D.J.F. and T.P.L.; funding acquisition, M.C.C. and T.P.L. All authors have read and agreed to the published version of the manuscript.

Funding: This work was supported by the National Institutes of Health (NIH) under the National Cancer Institute (NCI) Award Number P01 CA171983 (to T.P.L. and M.C.C.), NIH/NCI Cancer Center Support Grant P30 CA044579 (to T.P.L.), NIH/NCI Cancer Center Support Grant P30 CA138313 (to Z.M.S.), NIH/NCI F31 CA271809 (to J.U.), and NIH/NCI F99 CA284252 (to J.U.). This work was supported by the UVA Robert R. Wagner Fellowship (to J.U.) and Double Hoo Award (to J.U. and M.T.). This work was supported by the Veteran’s Administration via a Senior Research Career Scientist Award, IK6BX004603 (to C.E.C.). The content is solely the responsibility of the authors and does not necessarily represent the official views of the National Institutes of Health.

Institutional Review Board Statement: This study was conducted in accordance with the Declaration of Helsinki and approved by the Institutional Review Board of the University of Virginia (protocol code IRB-HSR #18445, 21625, 22123) and Penn State College of Medicine (Study ID: PRAMS029252EP, PRAMS040755EP).

Informed Consent Statement: Informed consent was obtained from all subjects involved in this study.

Data Availability Statement: Data will be made available upon request.

Acknowledgments: This work is dedicated in loving memory to Mark Kester. The authors thank those who provided cell lines for our studies: Dr. Francine Garrett-Bakelman, University of Virginia (F-36p and MOLM-16); Jacqueline Cloos and Carolien van Alphen, VU Medical Center Amsterdam (EOL-1, HEL, Kasumi-3, Kasumi-6, ME-1, ML2, MM-6, and NB4); Mark Levis, Johns Hopkins Medical Institutions (MOLM-13 and MOLM-14); Dr. Douglas Graham, Emory University (Nomo-1); Xiaorong Gu, Cleveland Clinic (OCI-AML2 and OCI-AML3); Harold L. Atkins, Ottawa Hospital Research Institute (OCI-AML4); Scott Kaufmann and Mithun Shah, Mayo Clinic (SET-2). We thank Galina Diakova and the UVA Biorepository and Tissue Research Facility (BTRF) (Research Resource Identifiers (RRID): SCR_022971) for providing primary AML patient samples and deidentified clinical data. The authors also acknowledge the contributions of the UVA ORIEN Team and the UVA BTRF in the consent of patients, specimen procurement, specimen processing, data abstraction, and providing access to molecular and clinical data (IRB-HSR #18445). We also thank James Norris, Medical University of South Carolina, for developing LCL-805.

Conflicts of Interest: D.J.F. has received research funding, honoraria, and/or stock options from AstraZeneca, Dren Bio, Recludix Pharma, and Kymera Therapeutics. T.P.L. has received Scientific Advisory Board membership, consultancy fees, honoraria, and/or stock options from Keystone Nano, Flagship Labs 86, Dren Bio, Recludix Pharma, Kymera Therapeutics, and Prime Genomics. M.C.C. owns shares in Keystone Nano. There are no conflicts of interest with the work presented in this manuscript. Other authors declare no competing interests. The funders had no role in the design of this study; in the collection, analyses, or interpretation of data; in the writing of this manuscript; or in the decision to publish the results.

References

1. Siegel, R.L.; Miller, K.D.; Jemal, A. Cancer statistics, 2020. *CA Cancer J. Clin.* **2020**, *70*, 7–30. [[CrossRef](#)] [[PubMed](#)]
2. De Kouchkovsky, I.; Abdul-Hay, M. Acute myeloid leukemia: A comprehensive review and 2016 update. *Blood Cancer J.* **2016**, *6*, e441. [[CrossRef](#)] [[PubMed](#)]
3. Sasaki, K.; Ravandi, F.; Kadia, T.M.; DiNardo, C.D.; Short, N.J.; Borthakur, G.; Jabbour, E.; Kantarjian, H.M. De novo acute myeloid leukemia: A population-based study of outcome in the United States based on the Surveillance, Epidemiology, and End Results (SEER) database, 1980 to 2017. *Cancer* **2021**, *127*, 2049–2061. [[CrossRef](#)] [[PubMed](#)]
4. Kantarjian, H.; Kadia, T.; DiNardo, C.; Daver, N.; Borthakur, G.; Jabbour, E.; Garcia-Manero, G.; Konopleva, M.; Ravandi, F. Acute myeloid leukemia: Current progress and future directions. *Blood Cancer J.* **2021**, *11*, 41. [[CrossRef](#)] [[PubMed](#)]
5. Bose, R.; Verheij, M.; Haimovitz-Friedman, A.; Scotto, K.; Fuks, Z.; Kolesnick, R. Ceramide synthase mediates daunorubicin-induced apoptosis: An alternative mechanism for generating death signals. *Cell* **1995**, *82*, 405–414. [[CrossRef](#)] [[PubMed](#)]
6. Deng, X.; Yin, X.; Allan, R.; Lu, D.D.; Maurer, C.W.; Haimovitz-Friedman, A.; Fuks, Z.; Shaham, S.; Kolesnick, R. Ceramide Biogenesis Is Required for Radiation-Induced Apoptosis in the Germ Line of *C. elegans*. *Science* **2008**, *322*, 110–115. [[CrossRef](#)]
7. Dany, M.; Gencer, S.; Nganga, R.; Thomas, R.J.; Oleinik, N.; Baron, K.D.; Szulc, Z.M.; Ruvolo, P.; Kornblau, S.; Andreeff, M.; et al. Targeting FLT3-ITD signaling mediates ceramide-dependent mitophagy and attenuates drug resistance in AML. *Blood* **2016**, *128*, 1944–1958. [[CrossRef](#)] [[PubMed](#)]
8. Senchenkov, A.; Litvak, D.A.; Cabot, M.C. Targeting Ceramide Metabolism—A Strategy for Overcoming Drug Resistance. *J. Natl. Cancer Inst.* **2001**, *93*, 347–357. [[CrossRef](#)]
9. Morad, S.A.F.; Cabot, M.C. Ceramide-orchestrated signalling in cancer cells. *Nat. Rev. Cancer* **2013**, *13*, 51–65. [[CrossRef](#)]
10. Kester, M.; Bassler, J.; Fox, T.E.; Carter, C.J.; Davidson, J.A.; Parette, M.R. Preclinical development of a C6-ceramide NanoLiposome, a novel sphingolipid therapeutic. *Biol. Chem.* **2015**, *396*, 737–747. [[CrossRef](#)]
11. Khokhlatchev, A.V.; Sharma, A.; Deering, T.G.; Shaw, J.J.P.; Costa-Pinheiro, P.; Golla, U.; Annageldiyev, C.; Cabot, M.C.; Conaway, M.R.; Tan, S.-F.; et al. Ceramide nanoliposomes augment the efficacy of venetoclax and cytarabine in models of acute myeloid leukemia. *FASEB J.* **2022**, *36*, e22514. [[CrossRef](#)] [[PubMed](#)]
12. Tan, S.-F.; Liu, X.; Fox, T.E.; Barth, B.M.; Sharma, A.; Turner, S.D.; Awwad, A.; Dewey, A.; Doi, K.; Spitzer, B.; et al. Acid ceramidase is upregulated in AML and represents a novel therapeutic target. *Oncotarget* **2016**, *7*, 83208–83222. [[CrossRef](#)] [[PubMed](#)]
13. Fisher-Wellman, K.H.; Kassai, M.; Hagen, J.T.; Neuffer, P.D.; Kester, M.; Loughran, T.P.; Chalfant, C.E.; Feith, D.J.; Tan, S.-F.; Fox, T.E.; et al. Simultaneous Inhibition of Ceramide Hydrolysis and Glycosylation Synergizes to Corrupt Mitochondrial Respiration and Signal Caspase Driven Cell Death in Drug-Resistant Acute Myeloid Leukemia. *Cancers* **2023**, *15*, 1883. [[CrossRef](#)] [[PubMed](#)]
14. Ung, J.; Tan, S.-F.; Fox, T.E.; Shaw, J.J.P.; Vass, L.R.; Costa-Pinheiro, P.; Garrett-Bakelman, F.E.; Keng, M.K.; Sharma, A.; Claxton, D.F.; et al. Harnessing the power of sphingolipids: Prospects for acute myeloid leukemia. *Blood Rev.* **2022**, *55*, 100950. [[CrossRef](#)] [[PubMed](#)]
15. Tan, S.-F.; Dunton, W.; Liu, X.; Fox, T.E.; Morad, S.A.F.; Desai, D.; Doi, K.; Conaway, M.R.; Amin, S.; Claxton, D.F.; et al. Acid ceramidase promotes drug resistance in acute myeloid leukemia through NF- κ B-dependent P-glycoprotein upregulation. *J. Lipid Res.* **2019**, *60*, 1078–1086. [[CrossRef](#)] [[PubMed](#)]
16. Kao, L.-P.; Morad, S.A.F.; Davis, T.S.; MacDougall, M.R.; Kassai, M.; Abdelmageed, N.; Fox, T.E.; Kester, M.; Loughran, T.P.; Abad, J.L.; et al. Chemotherapy selection pressure alters sphingolipid composition and mitochondrial bioenergetics in resistant HL-60 cells. *J. Lipid Res.* **2019**, *60*, 1590–1602. [[CrossRef](#)] [[PubMed](#)]
17. Tan, S.-F.; Pearson, J.M.; Feith, D.J.; Loughran, T.P. The emergence of acid ceramidase as a therapeutic target for acute myeloid leukemia. *Expert Opin. Ther. Targets* **2017**, *21*, 583–590. [[CrossRef](#)]
18. Govindarajah, N.; Clifford, R.; Bowden, D.; Sutton, P.A.; Parsons, J.L.; Vimalachandran, D. Sphingolipids and acid ceramidase as therapeutic targets in cancer therapy. *Crit. Rev. Oncol. Hematol.* **2019**, *138*, 104–111. [[CrossRef](#)]
19. Saied, E.M.; Arenz, C. Inhibitors of Ceramidases. *Chem. Phys. Lipids* **2016**, *197*, 60–68. [[CrossRef](#)]
20. Samsel, L.; Zaidel, G.; Drumgoole, H.M.; Jelovac, D.; Drachenberg, C.; Rhee, J.G.; Brodie, A.M.H.; Bielawska, A.; Smyth, M.J. The ceramide analog, B13, induces apoptosis in prostate cancer cell lines and inhibits tumor growth in prostate cancer xenografts. *Prostate* **2004**, *58*, 382–393. [[CrossRef](#)]
21. Selzner, M.; Bielawska, A.; Morse, M.A.; Rüdiger, H.A.; Sindram, D.; Hannun, Y.A.; Clavien, P.-A. Induction of Apoptotic Cell Death and Prevention of Tumor Growth by Ceramide Analogues in Metastatic Human Colon Cancer. *Cancer Res.* **2001**, *61*, 1233–1240. [[PubMed](#)]
22. Bai, A.; Szulc, Z.M.; Bielawski, J.; Pierce, J.S.; Rembiesa, B.; Terzieva, S.; Mao, C.; Xu, R.; Wu, B.; Clarke, C.J.; et al. Targeting (cellular) lysosomal acid ceramidase by B13: Design, synthesis and evaluation of novel DMG-B13 ester prodrugs. *Bioorg. Med. Chem.* **2014**, *22*, 6933–6944. [[CrossRef](#)] [[PubMed](#)]
23. McGrath, T.; Latoud, C.; Arnold, S.T.; Safa, A.R.; Felsted, R.L.; Center, M.S. Mechanisms of multidrug resistance in HL60 cells: Analysis of resistance associated membrane proteins and levels of mdr gene expression. *Biochem. Pharmacol.* **1989**, *38*, 3611–3619. [[CrossRef](#)] [[PubMed](#)]
24. Doi, K.; Liu, Q.; Gowda, K.; Barth, B.M.; Claxton, D.; Amin, S.; Loughran, T.P., Jr.; Wang, H.-G. Maritoclax induces apoptosis in acute myeloid leukemia cells with elevated Mcl-1 expression. *Cancer Biol. Ther.* **2014**, *15*, 1077–1086. [[CrossRef](#)] [[PubMed](#)]
25. Young, M.M.; Bui, V.; Chen, C.; Wang, H.-G. FTY720 induces non-canonical phosphatidylserine externalization and cell death in acute myeloid leukemia. *Cell Death Dis.* **2019**, *10*, 847. [[CrossRef](#)] [[PubMed](#)]

26. Vu, N.T.; Kim, M.; Stephenson, D.J.; MacKnight, H.P.; Chalfant, C.E. Ceramide Kinase Inhibition Drives Ferroptosis and Sensitivity to Cisplatin in Mutant KRAS Lung Cancer by Dysregulating VDAC-Mediated Mitochondria Function. *Mol. Cancer Res.* **2022**, *20*, 1429–1442. [[CrossRef](#)] [[PubMed](#)]
27. Ianevski, A.; Giri, A.K.; Aittokallio, T. SynergyFinder 2.0: Visual analytics of multi-drug combination synergies. *Nucleic Acids Res.* **2020**, *48*, W488–W493. [[CrossRef](#)]
28. Bedia, C.; Casas, J.; Garcia, V.; Levade, T.; Fabriàs, G. Synthesis of a Novel Ceramide Analogue and its Use in a High-Throughput Fluorogenic Assay for Ceramidases. *ChemBioChem* **2007**, *8*, 642–648. [[CrossRef](#)]
29. Gebai, A.; Gorelik, A.; Li, Z.; Illes, K.; Nagar, B. Structural basis for the activation of acid ceramidase. *Nat. Commun.* **2018**, *9*, 1621. [[CrossRef](#)]
30. Hartmann, D.; Lucks, J.; Fuchs, S.; Schiffmann, S.; Schreiber, Y.; Ferreirós, N.; Merkens, J.; Marschalek, R.; Geisslinger, G.; Grösch, S. Long chain ceramides and very long chain ceramides have opposite effects on human breast and colon cancer cell growth. *Int. J. Biochem. Cell Biol.* **2012**, *44*, 620–628. [[CrossRef](#)]
31. Fisher-Wellman, K.H.; Hagen, J.T.; Neufer, P.D.; Kassai, M.; Cabot, M.C. On the nature of ceramide-mitochondria interactions—Dissection using comprehensive mitochondrial phenotyping. *Cell. Signal.* **2021**, *78*, 109838. [[CrossRef](#)] [[PubMed](#)]
32. Taniai, T.; Shirai, Y.; Shimada, Y.; Hamura, R.; Yanagaki, M.; Takada, N.; Horiuchi, T.; Haruki, K.; Furukawa, K.; Uwagawa, T.; et al. Inhibition of acid ceramidase elicits mitochondrial dysfunction and oxidative stress in pancreatic cancer cells. *Cancer Sci.* **2021**, *112*, 4570–4579. [[CrossRef](#)] [[PubMed](#)]
33. Liu, F.; Li, X.; Lu, C.; Bai, A.; Bielawski, J.; Bielawska, A.; Marshall, B.; Schoenlein, P.V.; Lebedyeva, I.O.; Liu, K. Ceramide activates lysosomal cathepsin B and cathepsin D to attenuate autophagy and induces ER stress to suppress myeloid-derived suppressor cells. *Oncotarget* **2016**, *7*, 83907–83925. [[CrossRef](#)] [[PubMed](#)]
34. Taniguchi, M.; Ogiso, H.; Takeuchi, T.; Kitatani, K.; Umehara, H.; Okazaki, T. Lysosomal ceramide generated by acid sphingomyelinase triggers cytosolic cathepsin B-mediated degradation of X-linked inhibitor of apoptosis protein in natural killer/T lymphoma cell apoptosis. *Cell Death Dis.* **2015**, *6*, e1717. [[CrossRef](#)] [[PubMed](#)]
35. Paschall, A.V.; Zimmerman, M.A.; Torres, C.M.; Yang, D.; Chen, M.R.; Li, X.; Bieberich, E.; Bai, A.; Bielawski, J.; Bielawska, A.; et al. Ceramide targets XIAP and cIAP1 to sensitize metastatic colon and breast cancer cells to apoptosis induction to suppress tumor progression. *BMC Cancer* **2014**, *14*, 24. [[CrossRef](#)] [[PubMed](#)]
36. Holman, D.H.; Turner, L.S.; El-Zawahry, A.; Elojeimy, S.; Liu, X.; Bielawski, J.; Szulc, Z.M.; Norris, K.; Zeidan, Y.H.; Hannun, Y.A.; et al. Lysosomotropic acid ceramidase inhibitor induces apoptosis in prostate cancer cells. *Cancer Chemother. Pharmacol.* **2008**, *61*, 231–242. [[CrossRef](#)] [[PubMed](#)]
37. Glick, D.; Barth, S.; Macleod, K.F. Autophagy: Cellular and molecular mechanisms. *J. Pathol.* **2010**, *221*, 3–12. [[CrossRef](#)] [[PubMed](#)]
38. Mauthe, M.; Orhon, I.; Rocchi, C.; Zhou, X.; Luhr, M.; Hijlkema, K.-J.; Coppes, R.P.; Engedal, N.; Mari, M.; Reggiori, F. Chloroquine inhibits autophagic flux by decreasing autophagosome-lysosome fusion. *Autophagy* **2018**, *14*, 1435–1455. [[CrossRef](#)]
39. Mauvezin, C.; Neufeld, T.P. Bafilomycin A1 disrupts autophagic flux by inhibiting both V-ATPase-dependent acidification and Ca-P60A/SERCA-dependent autophagosome-lysosome fusion. *Autophagy* **2015**, *11*, 1437–1438. [[CrossRef](#)]
40. Ogretmen, B. Sphingolipid metabolism in cancer signalling and therapy. *Nat. Rev. Cancer* **2018**, *18*, 33–50. [[CrossRef](#)]
41. Zhang, X.; Kitatani, K.; Toyoshima, M.; Ishibashi, M.; Usui, T.; Minato, J.; Egiz, M.; Shigeta, S.; Fox, T.; Deering, T.; et al. Ceramide Nanoliposomes as a MLKL-Dependent, Necroptosis-Inducing, Chemotherapeutic Reagent in Ovarian Cancer. *Mol. Cancer Ther.* **2018**, *17*, 50–59. [[CrossRef](#)] [[PubMed](#)]
42. Estruch, M.; Reckzeh, K.; Vittori, C.; Centio, A.; Ali, M.; Engelhard, S.; Zhao, L.; Won, K.J.; Liu, P.; Porse, B.T.; et al. Targeted inhibition of cooperative mutation- and therapy-induced AKT activation in AML effectively enhances response to chemotherapy. *Leukemia* **2021**, *35*, 2030–2042. [[CrossRef](#)] [[PubMed](#)]
43. Emdal, K.B.; Palacio-Escat, N.; Wigerup, C.; Eguchi, A.; Nilsson, H.; Bekker-Jensen, D.B.; Rönnstrand, L.; Kazi, J.U.; Puissant, A.; Itzykson, R.; et al. Phosphoproteomics of primary AML patient samples reveals rationale for AKT combination therapy and p53 context to overcome selinexor resistance. *Cell Rep.* **2022**, *40*, 111177. [[CrossRef](#)] [[PubMed](#)]
44. Sophie, P.; Nicolas, C.; Jérôme, T.; Valérie, B.; Pascale, C.-L.; Lise, W.; Alexa, G.; Patrick, M.; Catherine, L.; Didier, B. Role of the PI3K/AKT and mTOR signaling pathways in acute myeloid leukemia. *Haematologica* **2010**, *95*, 819–828. [[CrossRef](#)]
45. Hawkins, C.C.; Jones, A.B.; Gordon, E.R.; Williford, S.E.; Harsh, Y.; Ziebro, J.K.; Landis, C.J.; Gc, S.; Crossman, D.K.; Cooper, S.J.; et al. Targeting Acid Ceramidase Inhibits Glioblastoma Cell Migration through Decreased AKT Signaling. *Cells* **2022**, *11*, 1873. [[CrossRef](#)] [[PubMed](#)]
46. Beckham, T.H.; Cheng, J.C.; Lu, P.; Shao, Y.; Troyer, D.; Lance, R.; Marrison, S.T.; Norris, J.S.; Liu, X. Acid ceramidase induces sphingosine kinase 1/S1P receptor 2-mediated activation of oncogenic Akt signaling. *Oncogenesis* **2013**, *2*, e49. [[CrossRef](#)] [[PubMed](#)]
47. Jo, H.; Mondal, S.; Tan, D.; Nagata, E.; Takizawa, S.; Sharma, A.K.; Hou, Q.; Shanmugasundaram, K.; Prasad, A.; Tung, J.K.; et al. Small molecule-induced cytosolic activation of protein kinase Akt rescues ischemia-elicited neuronal death. *Proc. Natl. Acad. Sci. USA* **2012**, *109*, 10581–10586. [[CrossRef](#)] [[PubMed](#)]
48. Rizzollo, F.; More, S.; Vangheluwe, P.; Agostinis, P. The lysosome as a master regulator of iron metabolism. *Trends. Biochem. Sci.* **2021**, *46*, 960–975. [[CrossRef](#)]
49. Zhu, Y.; Chang, B.; Pang, Y.; Wang, H.; Zhou, Y. Advances in Hypoxia-Inducible Factor-1 α Stabilizer Deferoxamine in Tissue Engineering. *Tissue Eng. Part B Rev.* **2022**, *29*, 347–357. [[CrossRef](#)]

50. Bai, A.; Mao, C.; Jenkins, R.W.; Szulc, Z.M.; Bielawska, A.; Hannun, Y.A. Anticancer actions of lysosomally targeted inhibitor, LCL521, of acid ceramidase. *PLoS ONE* **2017**, *12*, e0177805. [[CrossRef](#)]
51. Bai, A.; Bielawska, A.; Rahmaniyan, M.; Kravka, J.M.; Bielawski, J.; Hannun, Y.A. Dose dependent actions of LCL521 on acid ceramidase and key sphingolipid metabolites. *Biorg. Med. Chem.* **2018**, *26*, 6067–6075. [[CrossRef](#)] [[PubMed](#)]
52. Magliulo, D.; Bernardi, R. Hypoxic stress and hypoxia-inducible factors in leukemias. *Front. Oncol.* **2022**, *12*, 973978. [[CrossRef](#)] [[PubMed](#)]
53. Weber, S.; Parmon, A.; Kurrle, N.; Schnütgen, F.; Serve, H. The Clinical Significance of Iron Overload and Iron Metabolism in Myelodysplastic Syndrome and Acute Myeloid Leukemia. *Front. Immunol.* **2021**, *11*, 627662. [[CrossRef](#)]
54. Ciner, A.; Gourdin, T.; Davidson, J.; Parette, M.; Walker, S.J.; Fox, T.E.; Jiang, Y. A phase I study of the ceramide nanoliposome in patients with advanced solid tumors. *Cancer Chemother. Pharmacol.* **2023**. [[CrossRef](#)] [[PubMed](#)]
55. Chipuk, J.E.; McStay, G.P.; Bharti, A.; Kuwana, T.; Clarke, C.J.; Siskind, L.J.; Obeid, L.M.; Green, D.R. Sphingolipid Metabolism Cooperates with BAK and BAX to Promote the Mitochondrial Pathway of Apoptosis. *Cell* **2012**, *148*, 988–1000. [[CrossRef](#)]
56. Ganesan, V.; Perera, M.N.; Colombini, D.; Datskovskiy, D.; Chadha, K.; Colombini, M. Ceramide and activated Bax act synergistically to permeabilize the mitochondrial outer membrane. *Apoptosis* **2010**, *15*, 553–562. [[CrossRef](#)] [[PubMed](#)]
57. Lewis, A.C.; Pope, V.S.; Tea, M.N.; Li, M.; Nwosu, G.O.; Nguyen, T.M.; Wallington-Beddoe, C.T.; Moretti, P.A.B.; Anderson, D.; Creek, D.J.; et al. Ceramide-induced integrated stress response overcomes Bcl-2 inhibitor resistance in acute myeloid leukemia. *Blood* **2022**, *139*, 3737–3751. [[CrossRef](#)]

Disclaimer/Publisher’s Note: The statements, opinions and data contained in all publications are solely those of the individual author(s) and contributor(s) and not of MDPI and/or the editor(s). MDPI and/or the editor(s) disclaim responsibility for any injury to people or property resulting from any ideas, methods, instructions or products referred to in the content.